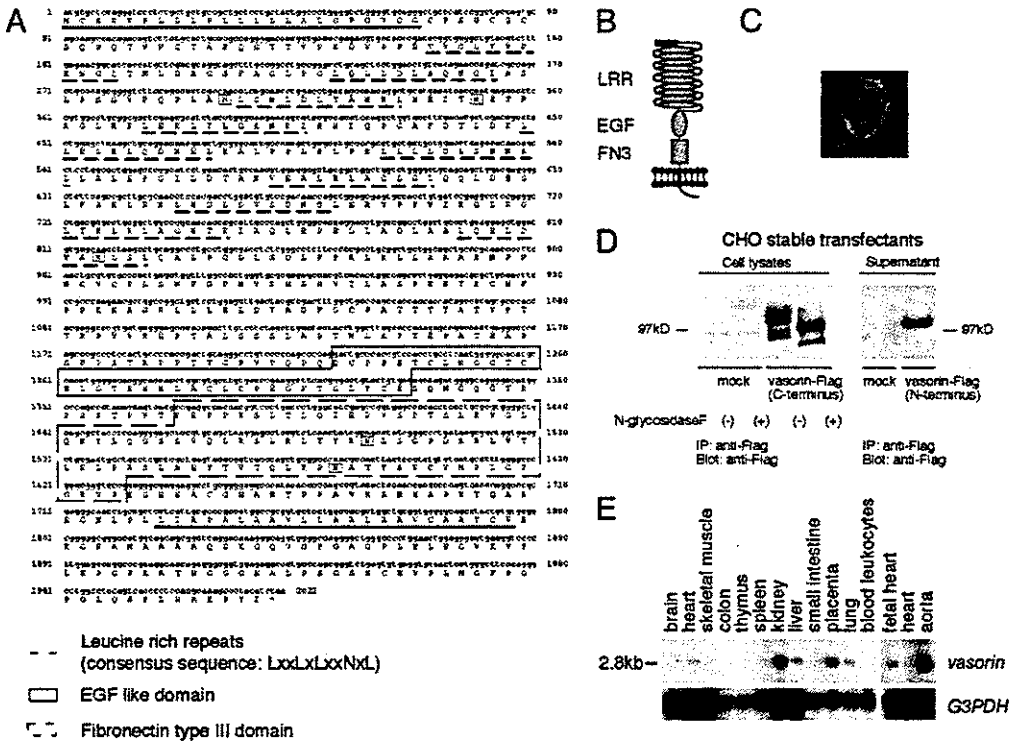

Fig. 1. Vasorin, an identified cell-surface protein. (*A*) Deduced amino acid sequence of human vasorin. The putative signal peptide (underlined), the LRRs (dotted underlines), the EGF motif (boxed), the fibronectin type III motif (dotted boxes), the transmembrane sequence (underlined), and five putative N-glycosylation sites (boxed) are indicated. (*B*) Structural model of vasorin. (*C*) Immunofluorescence analysis of subcellular localization of vasorin. Vasorin was expressed on the cell surface. (*D*) Cell lysates and supernatants of CHO cells stably expressing vasorin-Flag were subjected to immunoprecipitation and Western blot analysis by using an anti-Flag antibody. An ≈110-kDa protein for membrane-bound vasorin with C-terminal tag and a ≈100-kDa protein for soluble vasorin with N-terminal tag were detected under reducing conditions. N-glycosidase F treatment revealed that vasorin is N-glycosylated. (*E*) Northern blot analysis of adult human tissues. A single intense 2.8-kb band was detected and the strongest expression was observed in the aorta.

in *Supporting Text*, which is published as supporting information on the PNAS web site.

Production of the Recombinant Vasorin-Fc Chimera Protein. The bicistronic retroviral vector containing the *vasorin*-Fc chimera, pMX-*vasorin*-Fc chimera-IRES-EGFP, was constructed by inserting the cDNA for the whole-extracellular domain of human *vasorin* and the cDNA for the human Ig Fc region. CHO cells stably expressing the *vasorin*-Fc chimera were expanded in the medium supplemented with 2.5% Ultralow IgG FCS (Invitrogen) and 1% nonessential amino acids (Invitrogen). Secreted recombinant vasorin-Fc chimera protein was purified from the media of infected CHO cells by using Hitrap protein A columns (Amersham Biosciences).

Surface Plasmon Resonance Analysis. The BIAcoreTM2000 system (BIAcore, Uppsala) was used to characterize the interaction and to determine binding characteristics between the recombinant vasorin-Fc and TGF-β1, according to the manufacturer's instructions. To immobilize TGF-β1 on CM5 sensor chips, recombinant human TGF-β1 (R & D Systems) solution in 10 mM acetic acid (pH 4.0) was injected until the desired amount of coupled TGF-β1 was achieved, by using the standard amine-coupling procedure. All experiments were performed at room temperature by using the KINJECT command at a flow rate of 20 μl/min. Responses obtained on control chips were subtracted from those obtained on chips coupled with TGF-β1. Sensorgrams were analyzed by using BIAEVALUATION software (version 3.0).

Transient Transfection and Reporter Assay. CHO stable transfectants were transiently transfected with TGF-β1-responsive luciferase reporter plasmid (p3TP-lux) together with a β-galactosidase reporter plasmid driven by Rous sarcoma virus-LTR as an internal control, by using FuGENE6 (Roche Diagnostics, Roskilde, Denmark). After 24 h, the cells were stimulated for 24 h by adding TGF-β1 (R & D Systems) and were then assayed for luciferase and β-galactosidase activities. Experiments were performed several times and representative data are shown.

Rat Arterial Balloon-Injury Model. Adult rats (weighing 400–450 g) were anesthetized with chloral hydrate (370 mg/kg i.p.). Balloon denudation of the left common carotid artery was done by using a 2F Fogarty catheter (Baxter Edwards Healthcare, Irvine, CA), as described (6). The right common carotid artery served as a control. Rats were killed 3 or 14 days after injury, and the carotid arteries were perfused with 4% paraformaldehyde/PBS. Each injured left carotid artery was excised from the proximal edge of the omohyoid muscle to the carotid bifurcation. The middle third of the segment was isolated for subsequent analyses.

Generation of Recombinant Adenovirus (Ad) Expressing Vasorin. Replication-incompetent Ads expressing vasorin-Flag (Ad-vasorin) were prepared by using the Adeno-X system (Clontech) according to the manufacturer's instructions. Viral titer was measured by end-point dilution assay by using 293 cells.

Statistical Analysis. Quantitative values are expressed as the mean ± SD. Comparisons of means were made by using Student's *t* test for unpaired values; when >2 means were compared, an ANOVA with repeated measurements was used. If a significant *F* value was found, the Scheffé post hoc test for multiple comparisons was used to identify any differences among groups.

Results

Cloning of *Vasorin*. We screened a human heart cDNA library, by using SST-REX (ref. 3 and Table 1, which is published as supporting information on the PNAS web site), and identified a type I membrane protein of 673 aa (Fig. 1*A*). The extracellular region was composed of a putative hydrophobic signal sequence, 10 tandem arrays of a leucine-rich repeat (LRR), an epidermal growth factor (EGF)-like domain, and a fibronectin type III-like domain, and the short intracellular region contained no obvious signaling domain (Fig. 1 *A* and *B*). We termed this protein vasorin, based on the expression pattern described below. By using human vasorin as a probe, we identified homologous mouse and rat protein sequences in the EMBL/GenBank/DDBJ database (accession nos. AK012169 and XM 220168, respectively).

To observe the subcellular localization of vasorin, we stained CHO cells expressing human vasorin-Flag with an anti-Flag antibody (Fig. 1*C*), and confirmed this molecule to be expressed on the cell-surface membrane. Western blotting of cell lysates from CHO stable transfectants revealed a ≈110-kDa protein (Fig. 1*D*), which was larger than the predicted molecular mass. To determine whether this increase in molecular mass was due in part to N-linked glycosylation, immunoprecipitates of vasorin were treated with N-glycosydase F. An apparent shift in molecular mass of vasorin was observed, suggesting that vasorin is a cell-surface glycoprotein (Fig. 1*D*). Next, we examined the supernatant from CHO cells expressing human vasorin-Flag, and soluble vasorin was also detected (Fig. 1*D*).

***Vasorin* Is Predominantly Expressed in VSMCs.** Tissue distribution of *vasorin* was examined by using Northern blot analysis of adult human tissues. The highest expression was detected in the aorta, and moderate expression was detected in the kidney and placenta (Fig. 1*E*). We also performed Northern analysis of various human cell lines. Interestingly, *vasorin* was not expressed abundantly in any cell lines we examined (Fig. 6, which is published as supporting information on the PNAS web site).

To determine the expression pattern of *vasorin* within the aorta, we performed *in situ* hybridization analyses. By using the antisense probe, strong expression of *vasorin* was detected in the tunica media of the proximal ascending aorta (Fig. 2*A*), the descending thoracic aorta (Fig. 2*B*), the abdominal aorta (Fig. 2*C*), and the coronary arteries (Fig. 2 *E* and *F*), suggesting that *vasorin* is expressed in VSMCs of different origins. We also performed *in situ* hybridization analyses in the kidney. *Vasorin* expression was detected in interstitial cells (Fig. 2 *G* and *H*).

Developmental Regulation of *Vasorin* Expression. The developmental regulation of *vasorin* was investigated by using Northern blot and *in situ* hybridization analyses of staged mouse embryos. As shown in Fig. 3*A*, *vasorin* mRNA expression was detected in embryonic day (E)10.5 embryos, with increasing levels of expression observed at subsequent stages (E13.5 and E17.5). With *in situ* hybridization analyses, we examined the expression pattern of *vasorin* during aortic development (Fig. 3*B*). The expression of *vasorin* increased gradually in parallel with the differentiation of VSMCs in aortas at different stages of development (E11.5, E13.5, and E17.5).

When VSMCs are established in culture, a rapid transition from a contractile differentiated phenotype to a synthetic dedifferentiated phenotype occurs (5). To investigate the influence of this phenotypic modulation on the expression of *vasorin*, semiquantitative RT-PCR was performed to compare the expression of *vasorin* in the adult rat aorta with that in cultured rat aortic VSMCs. The expression of *vasorin* was significantly downregulated in the cultured VSMCs (Fig. 3*C*).

P19 embryonal carcinoma cells differentiate into SMCs when given retinoic acid (RA) treatment. Recently, this *in vitro* differentiation system was improved by generating stable cell lines of P19 carrying a smooth muscle α-actin promoter/puromycin resistance gene cassette to enrich SMC lineage cells, by using RA plus puromycin selection. One such stable line, designated as A404, shows a high propensity for SMC differentiation even before puromycin selection (7). As expected, *vasorin* gene expression was induced by RA-treatment in A404 cells (Fig. 3*D*).

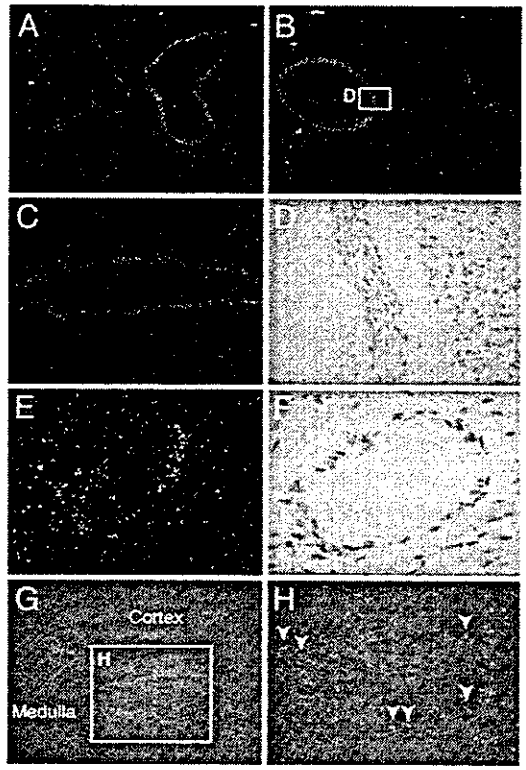

Fig. 2. *In situ* hybridization analysis of *vasorin*. Sections of adult mouse aorta at different levels (*A–D*), the coronary artery (*E* and *F*), and the kidney (*G* and *H*) are shown. *Vasorin* is expressed in VSMCs of different origins. White spots represent hybridization signals. (*A*) The proximal ascending aorta. (*B*) The descending thoracic aorta. (*C*) The abdominal aorta. (*D*) Partial magnification of bright-field image of *B*. Black spots within the elastic fibers represent hybridization signals. (*E*) The coronary artery. (*F*) A bright-field image of the coronary artery. Black spots represent hybridization signals. (*G*) The kidney. (*H*) Partial magnification of *G*. *Vasorin* is expressed in interstitial cells.

Vasorin Directly Binds to TGF-β and Modulates TGF-β Signaling *in Vitro*. An LRR, an EGF-like domain, and a fibronectin type III-like domain are characteristic motifs involved in protein–protein interactions (8). To clarify biological functions of vasorin, we generated recombinant vasorin-Fc fusion protein (Fig. 4*A*), and searched for binding partners of vasorin by using vasorin-Fc as a probe. When comparing the extracellular domain of vasorin with the EMBL/GenBank/DDBJ database, several other LRR protein family members, including decorin, were found to share a significant homology with vasorin. Decorin is a small leucine-rich proteoglycan that interacts directly with TGF-β (9, 10). Considering that vasorin has the same number of LRRs as decorin, and that TGF-β plays an important role in vascular pathophysiology, we tested whether TGF-β binds directly to vasorin. By using a surface plasmon resonance biosensor, we found that the extracellular domain of vasorin directly binds to TGF-β1 in a specific and significant manner (Fig. 4 *B* and *C*). The equilibrium dissociation constant (K_d) was calcu-

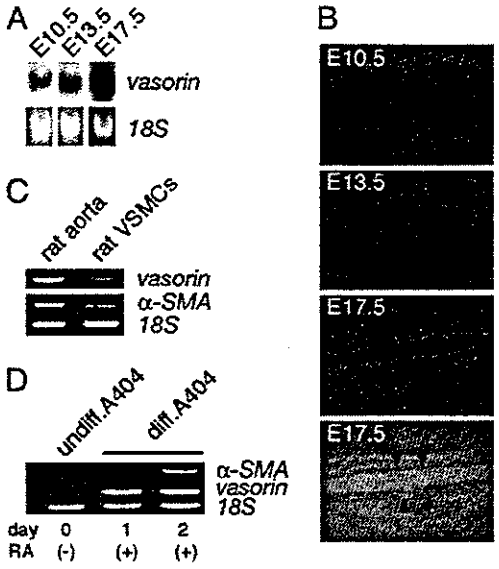

Fig. 3. Developmental regulation of *vasorin*. (*A*) Northern blot analysis of staged mouse embryos (E10.5, E13.5, and E17.5). (*B*) Expression pattern of *vasorin* during aortic development examined by *in situ* hybridization analyses. The fourth image is the corresponding bright-field image of the third representation. Arrowheads indicate the aorta in the mouse embryo (E17.5). (*C*) Semiquantitative RT-PCR comparing the expression of *vasorin* in the adult rat aorta with that in cultured rat aortic VSMCs. Rat α-smooth muscle actin (α-SMA) and 18S rRNA were used as a positive and an internal control, respectively. (*D*) Semiquantitative RT-PCR showing the induction of the *vasorin* gene in RA-treated A404 cells. Rat α-SMA and 18S rRNA were used as a positive and an internal control, respectively.

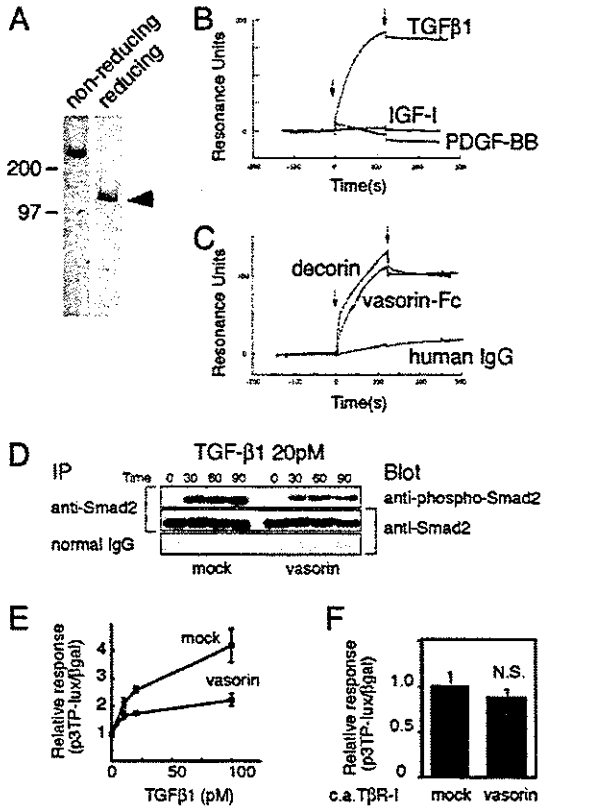

Fig. 4. Vasorin directly binds to TGF-β and modulates TGF-β signaling *in vitro*. (*A*) Purified recombinant vasorin-Fc fusion protein was free of protein contamination, as estimated by SDS/PAGE, followed by Coomassie blue staining. (*B*) Sensorgrams obtained from injection of vasorin-Fc on immobilized TGF-β1, PDGF-BB, and insulin-like growth factor I (IGF-I) are shown. (*C*) Sensorgrams obtained from injection of vasorin-Fc, decorin, and human IgG on immobilized TGF-β1 are shown. Arrowheads indicate initiation and termination of injections. (*D*) TGF-β-induced Smad2 phosphorylation was significantly inhibited in vasorin-expressing cells. Stable transfectants were treated with TGF-β1 (20 pM), and then immunoprecipitated with an anti-Smad2/3 antibody, followed by blotting with an anti-phospho-Smad2 antibody. (*E*) A reporter assay was performed by using the TGF-β-responsive reporter p3TP-lux. Stable transfectants were stimulated with TGF-β1 at various concentrations, and vasorin inhibited TGF-β-induced reporter gene activation. (*F*) Vasorin inhibited TGF-β signaling at the extracellular and/or cell-surface level. The p3TP-lux reporter and the constitutively active TβR-I were cotransfected into stable transfectants. Transfection of the constitutively active TβR-I activated the p3TP-lux reporter, but vasorin did not significantly inhibit this activation. N.S., not significant.

lated to be 0.86 nM. We also tested the binding of TGF-β2 and TGF-β3 to vasorin. TGF-β2 and TGF-β3 showed a specific binding to vasorin with a similar binding affinity to that of TGF-β1 (data not shown).

Next, we examined the functional role of vasorin in TGF-β signaling. First, stable transfectants expressing vasorin were stimulated by TGF-β1 (20 pM). Cells expressing vasorin showed a significant reduction in Smad2 phosphorylation (Fig. 4*D*). Second, we did a reporter assay, by using the TGF-β-responsive reporter p3TP-lux. TGF-β1 activated this reporter in a dose-dependent manner, and vasorin significantly inhibited this effect (Fig. 4*E*). This inhibitory effect of vasorin was specific to TGF-β signaling because vasorin did not affect the cellular responses to irrelevant cytokine stimulation (data not shown). Stable transfectants were also stimulated by using the constitutively active TGF-β type I receptor (constitutively active TβR-I) instead of TGF-β1 stimulation. Transfection of constitutively active TβR-I activated the p3TP-lux reporter, but vasorin did not significantly inhibit this activation (Fig. 4*F*). These findings indicate that vasorin inhibits TGF-β signaling at the extracellular and/or cell-surface level.

Vasorin Expression Was Down-Regulated During Vessel Repair After Arterial Injury, and Reversal of Vasorin Down-Regulation, by Using Ad-Mediated *in Vivo* Gene Transfer, Significantly Reduced Neointimal Formation at Least in Part by Modulating TGF-β Signaling in the Vessel Wall. To investigate *in vivo* functions of vasorin, we used a rat arterial balloon-injury model, because it is a well characterized atherosclerosis model of VSMC-derived lesions, and it is well established that TGF-β contributes to neointimal formation by promoting fibrosis.

Adult rats were subjected to balloon injury with a catheter inserted through the external carotid artery. Vascular injury provokes fibroproliferative activity in quiescent VSMCs, and the phenotypic modulation of VSMCs is induced. Because the fibroproliferative activity of VSMCs peaks at 3 days after injury (6), balloon-injured carotid arteries were harvested at 3 days after insertion to examine the expression levels of *vasorin* by semiquantitative RT-PCR. Consistent with our findings described above (Fig. 3 *A–D*), down-regulation of *vasorin* expression was induced by mechanical vascular injury (Fig. 5*A*). In contrast, the expression of several cytokines, including TGF-β, was up-regulated by vascular injury, and the ratio of TGF-β to vasorin was increased (Fig. 5*A*).

Next, we investigated the functional role of vasorin down-regulation in neointimal formation. To restore *vasorin* expression during vessel repair after injury, we did Ad-mediated *vasorin* gene transfer to balloon-injured rat carotid arteries. Replication-defective Ad-vasorin were constructed, and after denudation with a balloon catheter, the vessel wall was exposed to the adenoviral solution (1×10^9 pfu) for 20 min to deliver *vasorin* gene locally. First, arteries were harvested 3 days after-

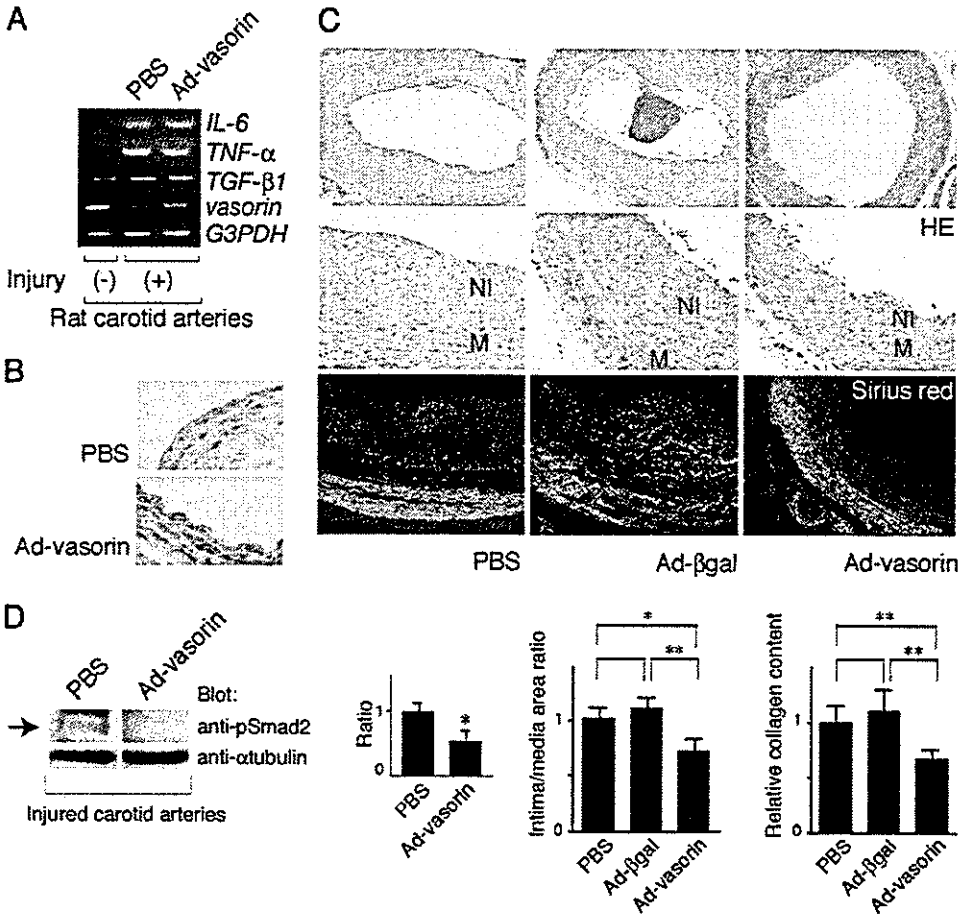

Fig. 5. Vasorin expression was down-regulated during vessel repair after arterial injury, and reversal of vasorin down-regulation significantly reduced neointimal formation, at least in part, by attenuating TGF-β signaling *in vivo*. (*A*) Rat carotid arteries were harvested at 3 days after injury to examine the expression levels of *vasorin* by semiquantitative RT-PCR analysis. Down-regulation of *vasorin* expression was induced by mechanical vascular injury, and Ad-vasorin treatment partially reversed this down-regulation. In contrast to vasorin, the expression of TGF-β1, TNF-α, and IL-6 was up-regulated by vascular injury and was not altered by vasorin administration. GAPDH was used as an internal control. (*B*) Vessels treated with Ad-vasorin were harvested 3 days afterward and were subjected to immunostaining to confirm protein expression by using the anti-Flag antibody. (*C*) Effects of Ad-vasorin on neointimal formation in rat carotid arteries at 14 days after injury ($n = 5$ arteries for each group). Representative hematoxylin/eosin-stained cross sections (*Top* and *Middle*) and Sirius red-stained cross sections (*Bottom*) of balloon-injured arteries treated with PBS (*Left*), Ad-β-galactosidase (*Center*), and Ad-vasorin (*Right*) are shown. (*Middle*) Partial magnifications of the respective *Top* images. Ad-vasorin administration significantly reduced the intima/media area ratio of injured arteries and collagen content in the lesions ($P < 0.01$), as compared with Ad-β-galactosidase administration. NI, neointima; M, media; HE, hematoxylin/eosin. *, $P < 0.05$; **, $P < 0.01$. (*D*) The inhibitory effects of vasorin administration on TGF-β signaling *in vivo*. Arteries were harvested 3 days after injury and were subjected to Western blot analysis by using the anti-phospho-Smad2 antibody. Representative data are shown. Smad2 phosphorylation was significantly reduced in all Ad-vasorin-treated arteries ($P < 0.05$). The blots were stripped and reprobed with the anti-α-tubulin antibody to ensure equal loading of proteins. The relative intensities of phospho-Smad2 bands were measured by densitometric scanning from three independent experiments. *, $P < 0.05$.

ward to examine the expression of vasorin by RT-PCR analysis (Fig. 5*A*), immunostaining (Fig. 5*B*), and Western blot analysis (data not shown). Ad-mediated *vasorin* gene transfer was successful (Fig. 5 *A* and *B*), and the expression of TGF-β, TNF-α, and IL-6 was not altered by vasorin administration (Fig. 5*A*). Second, arteries were harvested to assess the effect of *vasorin* gene transfer on neointimal formation ($n = 5$ arteries for each group) at 14 days after injury. The administration of Ad-vasorin significantly reduced the intima/media area ratio of injured arteries by 35% ($P < 0.01$), as compared with the administration of Ad-β-galactosidase (Fig. 5*C*), suggesting that restoration of vasorin expression had a significant inhibitory effect on neointimal formation. Because TGF-β stimulates extracellular matrix protein synthesis, and also functions as an antiinflammatory cytokine, we examined collagen content and leukocyte infiltration in the lesions quantitatively, by using Sirius red staining and CD45 staining, respectively. As shown in Fig. 5*C Lower*, vasorin administration significantly reduced collagen content in the lesions ($P < 0.01$), whereas leukocyte infiltration was not altered (data not shown).

Finally, we investigated whether *in vivo* vasorin administration inhibits TGF-β signaling in the vessel wall. Balloon-injured rat carotid arteries treated with Ad-vasorin were subjected to Western blot analysis, by using the anti-phospho-Smad2 antibody, when the fibroproliferative activity of VSMCs peaked (3 days after injury). Smad2 phosphorylation was significantly reduced in Ad-vasorin-treated arteries ($P < 0.05$; Fig. 5*D*). These results suggest that enhanced TGF-β signaling after vascular injury (Fig. 5*A*) is significantly inhibited by *in vivo* vasorin administration, and that vasorin inhibits neointimal formation at least in part by modulating TGF-β signaling in the vessel wall.

Discussion

VSMCs respond to various growth factors, and the best investigated situation in which VSMCs proliferate and produce extracellular matrix proteins *in vivo* is after vascular injury.

Whereas the rat carotid arterial balloon-injury model has been studied extensively, the underlying mechanisms that regulate vessel repair and neointimal formation appear to be the same in other arteries and in other species, including humans. The phenotype of VSMCs following arterial injury is similar to that observed during embryonic angiogenesis, and molecular mechanisms that regulate VSMC differentiation during embryonic development are thought to be recapitulated during vessel repair. *Vasorin* gene expression was developmentally regulated (Fig. 3 *A–D*), and, consistent with this finding, *vasorin* was down-regulated during vessel repair after arterial injury (Fig. 5*A*). This finding suggests its involvement in injury-induced vascular lesion formation. Therefore, we explored the *in vivo* functions of vasorin, by using a rat arterial balloon-injury model combined with Ad-mediated *in vivo* gene transfer. As shown in Fig. 5*C*, reversal of vasorin down-regulation had a significant inhibitory effect on neointimal formation. These results indicate that down-regulation of vasorin expression contributes to the fibroproliferative response to vascular injury.

Numerous factors that regulate VSMC activity have been studied in the arterial-injury model, and the results of these investigations suggest the importance of pathological extracellular stimuli, such as the renin-angiotensin system, catecholamines, EGF, platelet-derived growth factor (PDGF), insulin-like growth factor I, endothelin 1, TGF-β, and oxidative stress. TGF-β is a context-dependent pleiotropic cytokine, which plays a key role in the vascular response to injury. Several studies using gene transfer techniques have shown that locally enhanced TGF-β signaling enables matrix-rich neointima to develop in uninjured normal arteries of rats (11, 12). In contrast, localized blockade of TGF-β signaling results in the inhibition of neointimal formation, accompanied by reduced extracellular matrix synthesis in a rat balloon-injury model (13, 14). Of clinical relevance is the observation that the expression levels of TGF-β mRNA in restenotic lesions are higher than those in primary atherosclerotic lesions (15). These investigations indicate that TGF-β functions as a fibrogenic cytokine in a balloon-injury model, and apparently aggravates neointimal formation by promoting fibrosis. In this paper, we found that vasorin directly binds to TGF-β and negatively modulates TGF-β signaling in the vessel wall (Figs. 4 and 5*D*). Considering the functional role of TGF-β in this model, it is reasonably assumed that the *in vivo* phenotype induced by Ad-vasorin administration is mediated at least in part by the inhibitory effects of vasorin on TGF-β signaling in the vessel wall.

The extracellular region of vasorin is composed of ten tandem arrays of an LRR, an EGF-like domain, and a fibronectin type III-like domain, that are known to be involved in protein–protein interactions (Fig. 1*B*). Secreted and cell-surface molecules containing those domains, such as extracellular matrix proteins and adhesion molecules, sometimes have multiple binding partners. PDGF and TGF-β are prominent growth factors that have been suggested to play an important role in neointimal formation after arterial injury, and we demonstrated here that vasorin directly binds to TGF-β, but not to PDGF (Fig. 4*B*). However, it is possible that vasorin has other binding partners and that vasorin affects not only TGF-β signaling but also other signaling pathways, through another yet-to-be-identified mechanism. Further investigations will be needed to clarify these issues.

In the present study, we found that down-regulation of vasorin expression was induced by acute vascular injury, and that reversal of vasorin down-regulation during vessel repair inhibits neointimal formation, at least in part, by modulating cellular responses to TGF-β. These data raise a possibility that the gene expression profile of cell-surface molecules is changed by mechanical vascular injury, and that altered cellular responses to growth factors in dedifferentiated VSMCs are in part due to this change. Thus, identification and modification of the pivotal gene expression of cell-surface molecules in VSMCs may be a potential therapeutic approach to vascular fibroproliferative disorders.

We thank Dr. G. K. Owens for A404 cells, M. Ohara for language assistance, and Drs. H. Ono and H. Ogasawara for valuable advice. This work was also supported in part by grants from the Ministry of Education, Science, Technology, Sports, and Culture of Japan. The Division of Hematopoietic Factors was supported in part by the Chugai Pharmaceutical Company, Ltd.

1. Tashiro, K., Tada, H., Heilker, R., Shirozu, M., Nakano, T. & Honjo, T. (1993) *Science* **261**, 600–603.
2. Klein, R. D., Gu, Q., Goddard, A. & Rosenthal, A. (1996) *Proc. Natl. Acad. Sci. USA* **93**, 7108–7113.
3. Kojima, T. & Kitamura, T. (1999) *Nat. Biotechnol.* **17**, 487–490.
4. Nosaka, T., Kawashima, T., Misawa, K., Ikuta, K., Mui, A. L. & Kitamura, T. (1999) *EMBO J.* **18**, 4754–4765.
5. Chamley-Campbell, J., Campbell, G. R. & Ross, R. (1979) *Physiol. Rev.* **59**, 1–61.
6. Clowes, A. W., Reidy, M. A. & Clowes, M. M. (1983) *Lab. Invest.* **49**, 327–333.
7. Manabe, I. & Owens, G. (2001) *Circ. Res.* **88**, 1127–1134.
8. Kajava, A. V. (1998) *J. Mol. Biol.* **277**, 519–527.
9. Iozzo, R. V. (1999) *J. Biol. Chem.* **274**, 18843–18846.
10. Yamaguchi, Y., Mann, D. M. & Ruoslahti, E. (1990) *Nature* **346**, 281–284.
11. Nabel, E. G., Shum, L., Pompili, V. J., Yang, Z. Y., San, H., Shu, H. B., Liptay, S., Gold, L., Gordon, D., Derynck, R., *et al.* (1993) *Proc. Natl. Acad. Sci. USA* **90**, 10759–10763.
12. Schulick, A. H., Taylor, A. J., Zuo, W., Qiu, C. B., Dong, G., Woodward, R. N., Agah, R., Roberts, A. B., Virmani, R. & Dichek, D. A. (1998) *Proc. Natl. Acad. Sci. USA* **95**, 6983–6988.
13. Yamamoto, K., Morishita, R., Tomita, N., Shimozato, T., Nakagami, H., Kikuchi, A., Aoki, M., Higaki, J., Kaneda, Y. & Ogihara, T. (2000) *Circulation* **102**, 1308–1314.
14. Kingston, P. A., Sinha, S., David, A., Castro, M. G., Lowenstein, P. R. & Heagerty, A. M. (2001) *Circulation* **104**, 2595–2601.
15. Nikol, S., Isner, J. M., Pickering, J. G., Kearney, M., Leclerc, G. & Weir, L. (1992) *J. Clin. Invest.* **90**, 1582–1592.

Human Molecular Genetics, 2004, Vol. 13, No. 2 **151–157**
DOI: 10.1093/hmg/ddh014
Advance Access published on November 25, 2003

Overexpression of P104L mutant caveolin-3 in mice develops hypertrophic cardiomyopathy with enhanced contractility in association with increased endothelial nitric oxide synthase activity

Yutaka Ohsawa[1], Haruhiro Toko[2], Masashi Katsura[3], Kazue Morimoto[1], Haruki Yamada[1], Yaeko Ichikawa[1], Tatsufumi Murakami[1], Seitaro Ohkuma[3], Issei Komuro[2] and Yoshihide Sunada[1,*]

[1]Division of Neurology, Department of Internal Medicine, Kawasaki Medical School, 577 Matsushima, Kurashiki-City, Okayama 701-0192, Japan, [2]Department of Cardiovascular Science and Medicine, Chiba University Graduate School of Medicine, 1-8-1 Inohana, Chuo-ku, Chiba 260-8670, Japan and [3]Department of Pharmacology, Kawasaki Medical School, 577 Matsushima, Kurashiki-City, Okayama 701-0192, Japan

Received July 8, 2003; Revised and Accepted November 11, 2003

The effect of endogenous nitric oxide synthase (NOS) on cardiac contractility and architecture has been a matter of debate. A role for NOS in cardiac hypertrophy has recently been demonstrated by studies which have shown hypertrophic cardiomyopathy (HCM) with altered contractility in constitutive NOS (cNOS) knockout mice. Caveolin-3, a strong inhibitor of all NOS isoforms, is expressed in sarcolemmal caveolae microdomains and binds to cNOS *in vivo*: endothelial nitric oxide synthase (eNOS) in cardiac myocytes and neuronal nitric oxide synthase (nNOS) in skeletal myocytes. The current study characterized the biochemical and cardiac parameters of P104L mutant caveolin-3 transgenic mice, a model of an autosomal dominant limb-girdle muscular dystrophy (LGMD1C). Transgenic mouse hearts demonstrated HCM, enhanced basal contractility, decreased left ventricular end diastolic diameter, and loss and cytoplasmic mislocalization of caveolin-3 protein. Surprisingly, cardiac muscle showed activation of eNOS catalytic activity without increased expression of all NOS isoforms. These data suggest that a moderate increase in eNOS activity associated with loss of caveolin-3 results in HCM.

INTRODUCTION

Caveolae are 50–100 nm flask-shaped invaginations of the plasma membrane that are primarily composed of the 21–24 kDa integral membrane proteins, caveolin-1, -2 and -3 (1). These structures participate in vesicular trafficking events and signal transduction by acting as scaffold proteins for specific lipids and lipid-modified signaling molecules (e.g. cholesterol, G-proteins, G-protein coupled receptors, receptor tyrosine kinases and nitric oxide synthase) (2–4).

Caveolin-3 is a myocyte-specific isoform that assembles to ~350 kDa homo-oligomers in the sarcoplasmic reticulum (SR) (2). Caveolin-3 homo-oligomers are translocated to the plasma membrane via the trans-Golgi network (2,4) and inhibit all NOS isoforms *in vitro* and bind to constitutive NOS (cNOS) *in vivo*: endothelial nitric oxide synthase (eNOS) in cardiac myocytes and neuronal nitric oxide synthase (nNOS) in skeletal myocytes (5–8).

Autosomal dominant limb-girdle muscular dystrophy 1C (LGMD1C) and autosomal dominant rippling muscle disease (AD-RMD) result from heterozygous mutations of the skeletal muscle caveolin-3 gene (*CAV3*) (9,10). We previously generated transgenic (Tg) mice (TgCAV3M1 mice) with severe myopathy secondary to overexpression of P104L mutant caveolin-3 as a model of LGMD1C (11). Further study of this transgenic animal model revealed increased sarcolemmal nNOS activity without alternations of nNOS expression at both mRNA and protein levels. Other reports demonstrated that caveolin-3 is down-regulated in the hypertrophic hearts of spontaneously hypertensive rats (12) and that circulatory NO

*To whom correspondence should be addressed: Tel: +81 864621111; Fax: +81 864621199; Email: ysunada@med.kawasaki-m.ac.jp

Human Molecular Genetics, Vol. 13, No. 2 © Oxford University Press 2004; all rights reserved

(13) or eNOS mRNA in cardiac muscle (14) increases in human heart failure. These observations suggest that loss of caveolin-3 may modulate cardiac architecture and function via disinhibition of NOS activity. The present study investigated this hypothesis by characterizing the biochemical and cardiac parameters of TgCAV3M1 mice.

RESULTS

TgCAV3M1 mice show hypertrophic cardiomyopathy with enhanced contractility

TgCAV3M1 mice were generated as described previously (11). Tg mice showed poor growth and were significantly smaller than their wild-type (Wt) littermates at 4, 12, 24 and 36 weeks of age (Fig. 1A) and demonstrated kyphosis of the spine and paralysis of the hindlimbs from 12 weeks of age. The Tg mice exhibited increased cardiac weight and statistically significant increases in the cardiac weight-to-body weight ratio at 4, 12, 24 and 36 weeks of age when compared with their Wt littermates (Fig. 1B and C). However, from the clinical standpoint, the Tg mice have so far not developed any significant symptoms of heart failure, nor have any significant differences in life span been observed between the Wt and Tg mice.

Gross appearance of the hearts from 6-week-old Wt and Tg mice at the lower ventricular level showed thickening of the interventricular septum and the posterior wall of the left ventricle, resulting in a smaller left ventricular chamber in the Tg mice (Fig. 2A). Hematoxylin and eosin staining of cardiac muscle sections showed hypertrophy of cardiac myofibers in the Tg mice (Fig. 2B). The diameters of 1000 cardiac muscle fibers from five Tg mice and five Wt mice, respectively, were measured. The frequency distribution (percentage) of the cardiac myofiber diameter in Tg mice showed a distribution skew to the right and marked size variability on both longitudinal and transverse sections when compared to Wt mice (Fig. 2C). The mean cardiac muscle fiber diameter and standard deviation were significantly larger ($P < 0.05$) in Tg mice (8.53 ± 1.43 μm on longitudinal section and 9.35 ± 1.17 μm on transverse sections) than in Wt mice (6.55 ± 0.91 and 7.32 ± 0.83 μm, respectively; Fig. 2C). Gene expression of cardiac myocyte hypertrophic markers, atrial natriuretic peptide (ANP) and brain-derived natriuretic peptide (BNP) was analyzed by northern blotting. Densitometry using BAS2000 Image Analyzer demonstrated that both the ANP and BNP transcripts in the Tg mouse hearts were up-regulated by 1.69- and 1.54-fold, respectively (Fig. 2D). Transthoracic echocardiogram performed in 24-week-old Tg mice ($n = 7$) revealed unique pathophysiological characteristics for HCM; increased thickness of the interventricular septum and left ventricular posterior wall, hypercontractility (increased left ventricular fractional shortening) and diastolic dysfunction (decreased left ventricular end diastolic diameter; Table 1).

Tg CAV3M1 mouse hearts show loss and cytoplasmic mislocalization of caveolin-3

Northern blot analysis of Tg mouse cardiac muscle showed overexpression of smaller-sized (~1.1 kb) mutant caveolin-3

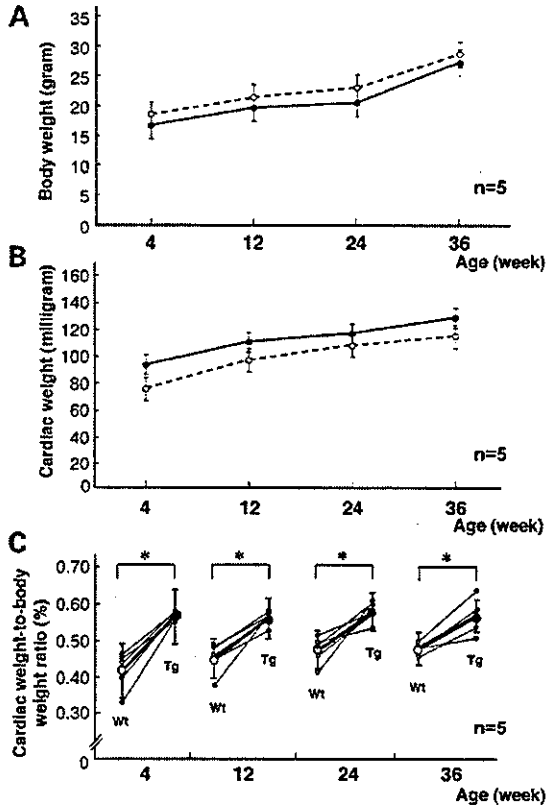

Figure 1. Comparison of body weight (**A**), cardiac weight (**B**) and the cardiac weight-to-body weight ratio (**C**) between Wt (open circle, $n = 5$) and Tg (solid circle, $n = 5$) mice at 4, 12, 24 and 36 weeks of age. Note that the smaller body weight and larger cardiac weight in the Tg mice results in statistically significant increases in the mean cardiac weight-to-body weight ratios. Error bars are ±SD. *Statistical significance was determined by *Welch's t*-test ($P < 0.05$).

mRNA (Fig. 3A). Detection of endogenous caveolin-3 mRNA (~1.4 kb) in the Tg mice was interfered with by an excessive amount of the mutant caveolin-3 mRNA. Then, the differential expression of endogenous and mutant caveolin-3 mRNA was analyzed by RT–PCR using two distinct reverse primers as described previously (11). RT–PCR confirmed the expression of endogenous caveolin-3 mRNA in Tg mouse hearts as well as in Wt mouse hearts, as shown in Figure 3B.

In sharp contrast to overexpression of mutant caveolin-3 mRNA, immunoblot analysis showed a marked reduction (~95%) of caveolin-3 protein in Tg mouse cardiac muscle (Fig. 3C). Immunohistochemical analysis demonstrated sarcolemmal localization of caveolin-3 protein in the Wt mice, while the majority of cardiac muscle fibers of the Tg mice showed only weak sarcolemmal immunoreactivity with small, cytoplasmic, dot-like immunoreactivity (Fig. 3D). There was no change in sarcolemmal dystrophin expression in the Tg mice (Fig. 3D). Caveolin-1 was expressed in endothelial cells and showed no compensatory overexpression in Tg mouse cardiac myocytes (Fig. 3D). β-Dystroglycan expression was similar in the Wt and Tg mice (Fig. 3C).

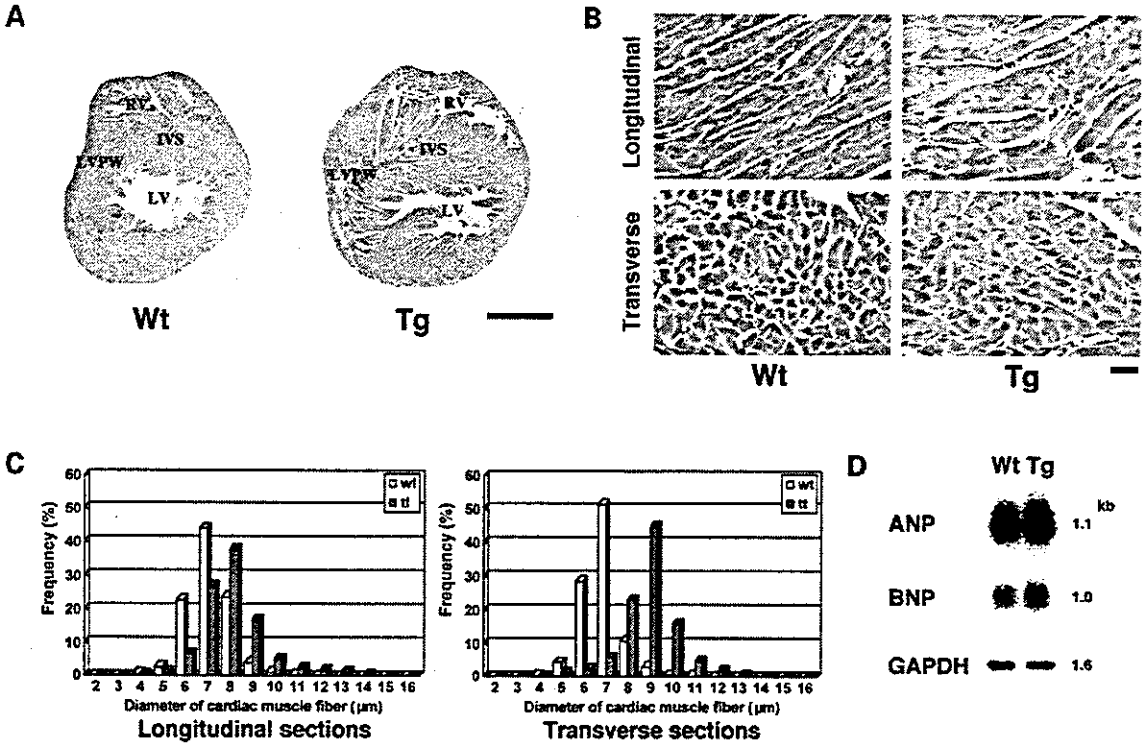

Figure 2. Histology of hearts from 6-week-old Wt and Tg mice. (**A**) Gross appearance of transverse lower ventricular sections from Wt and Tg mouse hearts. Note that apparent thickening of the interventricular septum and posterior wall of the left ventricle results in a tiny ventricular chamber in the Tg mouse heart (right). LV, left ventricle; IVS, interventricular septum; LVPW, left ventricular posterior wall; RV, right ventricle. Bar, 1 mm. (**B**) H&E staining of cardiac muscle sections from 6-week-old Wt or Tg mice. Note the myofiber hypertrophy in the Tg mouse hearts in both longitudinal (Upper panels) and transverse (lower panels) sections. Bar, 10 μm. (**C**) Histogram of cardiac myofiber diameter from 6-week-old Wt or Tg mice on longitudinal sections (left) and on transverse sections (right). The diameters of 1000 cardiac muscle fibers from five Tg mice and five Wt mice were measured. Note that the frequency distribution (%) of the cardiac muscle fiber diameter in the Tg mice compared with that in the Wt mice shows a skewed distribution to the right and marked size variability, thus indicating cardiac myocyte hypertrophy. The diameter of each cardiac muscle fiber was measured by the IBAS 2000 image analysis system (Zeiss). (**D**) Northern blot analysis of cardiac myocyte hypertrophic markers; ANP and BNP. Radiointensities of ANP and BNP transcripts in the Tg mouse hearts were up-regulated by 1.69- and 1.54-fold, respectively.

Table 1. Transthoracic echocardiographic analysis of hearts from 24-week-old Wt and Tg mice

Group	Interventricular septal thickness (mm)	Left ventricular posterior wall thickness (mm)	Left ventricular end diastolic diameter (mm)	Left ventricular end systolic diameter (mm)	Left ventricular fractional shortening (%)
Wt	0.83 ± 0.11	0.78 ± 0.08	3.94 ± 0.28	2.14 ± 0.23	45.60 ± 4.00
Tg	1.04 ± 0.12*	1.07 ± 0.11*	3.00 ± 0.30*	1.15 ± 0.18*	61.20 ± 4.70*

*$P < 0.01$. Wt ($n = 7$); Tg ($n = 7$).

NOS activity is increased in TgCAV3M1 mouse hearts

Expression of all NOS isoforms was similar when Wt and Tg mice cardiac muscles were compared by northern blot and immunoblot analyses (Fig. 4A and B). In addition, sub-sarcolemmal and vascular endothelial localization of eNOS was similar in Tg and Wt mouse hearts (Fig. 4C). NOS activity was quantified in crude extracts from freshly isolated hearts from six-week-old Wt and Tg mice ($n = 8$). Total NOS and eNOS activities in the Tg mouse hearts were significantly higher ($P < 0.05$) than those in the Wt mouse hearts: total NOS activity (pmol/mg protein/min)—Tg mouse, 5.10 ± 0.32, Wt mouse, 3.38 ± 0.32; eNOS activity (pmol/mg protein/min)—Tg mouse, 4.03 ± 0.32, Wt mouse, 2.31 ± 0.24. No significant differences were observed in either nNOS activity (pmol/mg protein/min)—Tg mouse, 0.77 ± 0.07, Wt mouse, 0.75 ± 0.06—or iNOS activity (pmol/mg protein/min)—Tg mouse, 0.30 ± 0.02, Wt mouse, 0.31 ± 0.03 (Fig. 4D).

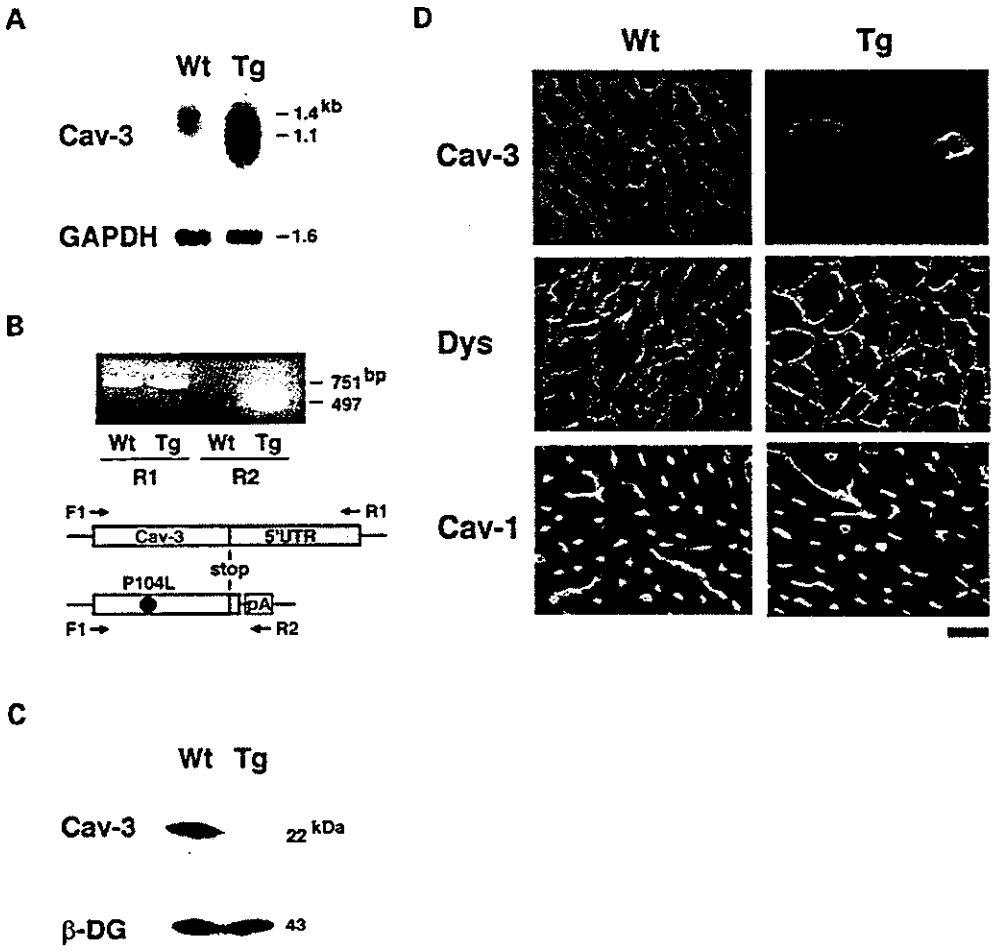

Figure 3. (A) Northern blot analysis of caveolin-3 in cardiac muscle from 6-week-old Wt and Tg mice. The smaller-sized (~1.1 kb) mutant caveolin-3 mRNA was expressed excessively in the Tg mice compared with the Wt mice. (B) RT–PCR analysis of endogeneous or mutant caveolin-3 in cardiac muscle from 6-week-old Wt and Tg mice. The endogenous caveolin-3 was detectable in Tg mice as well as Wt mice using primers of F1/R1 (upper panel, left). The mutant caveolin-3 mRNA was detectable only in Tg mice using primers of F1/R2 (upper panel, right). R1 corresponds to the 5′-untranslated region (5′-UTR) of the caveolin-3 transcript, whereas R2 corresponds to the SV40 polyadenylation site (pA) of the transgene transcript (lower panel). (C) Immunoblot analysis of caveolin-3 in total protein extracts from 6-week-old Wt and Tg mouse cardiac muscles. Caveolin-3 expression was markedly reduced in the Tg mice. In contrast, β-DG expression was similar in the Wt and Tg mice. (D) Immunohistochemical analysis of cardiac muscle from 6-week-old Wt and Tg mice. Lower ventricular cryosections from the Wt and Tg mice were stained with antibodies against caveolin-3 (Cav-3), dystrophin (Dys) and caveolin-1 (Cav-1). Caveolin-3 localized to the sarcolemma in the Wt mice, but the Tg mice generally lacked caveolin-3 except for a few fibers that showed weak cytoplasmic localization of caveolin-3. The expression of dystrophin and caveolin-1 was similar in the Wt and Tg mice. Bar, 10 μm.

DISCUSSION

Caveolin-3 is a strong physiological inhibitor of NOS and expressed specifically in cardiac and skeletal myocytes (5–8). The present study demonstrated the occurrence of hypertrophic cardiomyopathy with enhanced contractility in association with increased eNOS activity in caveolin-3-deficient transgenic mice without changes in NOS expression. Therefore, loss of NOS inhibition secondary to deficient caveolin-3 may contribute to the pathogenesis of hypertrophic cardiomyopathy.

NOS activity may modulate cardiac contractility and architecture (15–18). eNOS is localized in caveolae (5,8) and plays a role in inhibition of β-adrenergic-induced contractility (19,20). NO generated by eNOS may also interact with the SR ryanodine receptor (21). In contrast, nNOS, located in the SR (15,22), increases SR Ca^{2+} release and enhances cardiac contractility (15,23). eNOS knockout mice show enhanced contractility (15), while overexpression of eNOS results in reduced cardiac size and contractility (24). Unexpectedly, our Tg mouse hearts with moderately increased eNOS activity showed enhanced

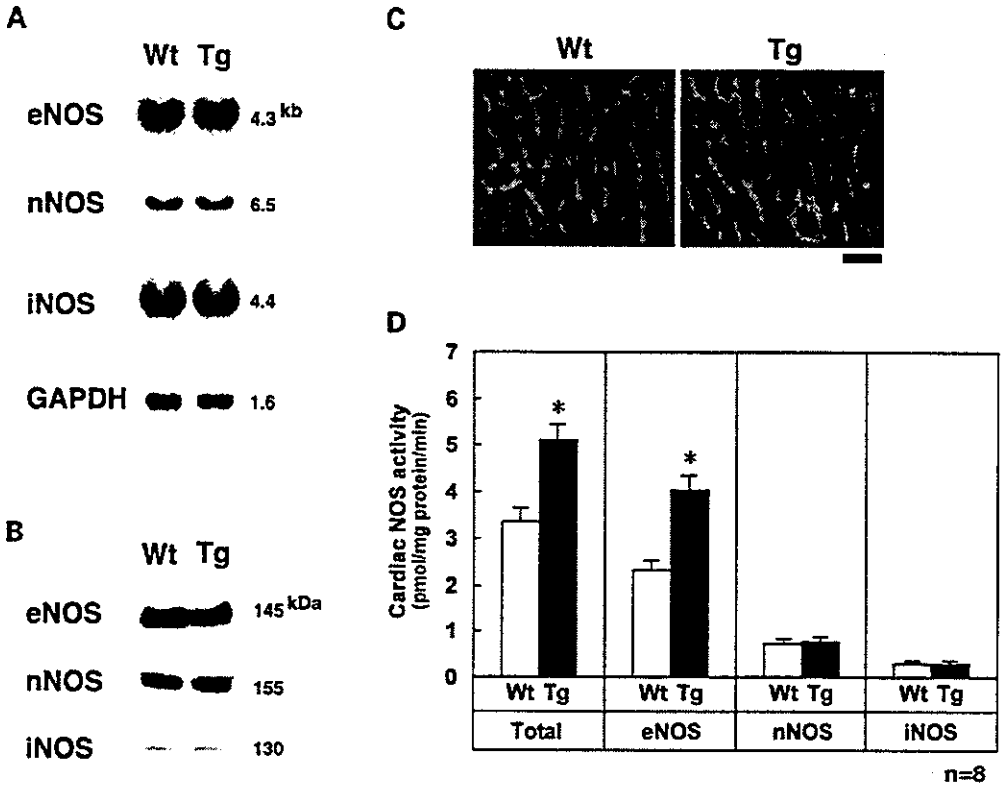

Figure 4. Northern blot analysis (**A**) and immunoblot analysis (**B**) of NOS isoforms in cardiac muscle from 6-week-old Wt and Tg mice. Note the comparable expression of all NOS isoforms in the Wt and Tg mice. (**C**) Immunohistochemical analysis of eNOS in cardiac muscle from 6-week-old Wt and Tg mice. The expression pattern of eNOS was similar in the Wt and Tg mice. Bar, 10 μm. (**D**) NOS activities in crude extracts from cardiac muscle from 6-week-old Wt and Tg mice. Note that significant increases in total NOS and eNOS activity were observed in the Tg mice, compared to the Wt mice ($n = 8$). In contrast no significant difference was observed in either nNOS or iNOS activity between the Tg and Wt mice. Data are expressed as mean ± SD. *Statistical significance was determined using Welch's *t*-test ($P < 0.05$).

contractility and hypertrophic cardiomyopathy. It is noteworthy that exogenous NO, derived from pharmacological NO donors, produces a biphasic contractile response in cardiac tissue with augmentation at low NO levels and depression at high NO levels (25–27). Based on these exogenous NO donor experiments, we postulate that a moderate activation of eNOS activity, as seen in the mutant caveolin-3 Tg mouse hearts enhances contractility and leads to hypertrophic cardiomyopathy, whereas an extremely high activation of eNOS activity, as seen in mouse hearts in which eNOS is overexpressed, reduces contractility and cardiac size.

Woodman *et al.* (28) reported that caveolin-3 null mice showed cardiomyopathy and suppressed contractility, possibly secondary to alterations in the p42/44 MAPK pathway, but they did not characterize changes in NOS isoform profiles. Based on previous studies and the present data, we would predict greater NOS activity in caveolin-3 null mouse hearts than in the hearts of mutant caveolin-3 transgenic mice. This higher NOS activity in caveolin-3 null mouse hearts may result in suppression of cardiac contractility.

To date hypertrophic cardiomyopathy has not been reported in LGMD1C patients. However, in only one German pedigree of autosomal dominant rippling muscle disease (AD-RMD) (29), which was proven to carry a caveolin-3 missense mutation (A45V) (10), two patients died suddenly of possible cardiac arrhythmia. An autopsy study of one patient in this pedigree disclosed non-obstructive cardiomyopathy, which was poorly described (29). Cardiac involvement, cardiomyopathy and/or arrhythmia may be a rare but possible feature of CAV-3 missense mutations. Further extensive clinical examination of cardiac function in LGMD1C patients is necessary to test this possibility. Furthermore, it is plausible that the higher copy number of the mutant caveolin-3 gene in TgCAV3M1 mice promotes a disease process leading to HCM.

In conclusion, we propose that moderate eNOS activation caused by loss of caveolin-3 may be involved in a caveolin-3-mediated hypertrophic signal pathway of cardiac myocytes.

MATERIALS AND METHODS

RT–PCR

cDNA templates were reverse-transcribed from 1 μg of total RNA from mouse cardiac muscle, primed with an oligo(dT)$_{12-18}$

primer and then subjected to PCR. For amplification of the endogenous caveolin-3 gene, we used F1 (5′-CCCAGCCTCACAAT GATGACCGAAG-3′) and R1 (5′-CATGTGAACGCAAAGCC TTGC-3′). For amplification of the transgene, we used F1 and R2 (5′-GCATTCTAGTTGTGGTTT-3′). As illustrated in Figure 3B, R1 and R2 correspond to the 5′-untranslated region of caveolin-3 cDNA and the SV40 polyadenylation site, respectively, as described previously (11).

Northern blot analysis

RT–PCR product of endogenous caveolin-3 was subcloned into TA vector pCR2.1 (Invitrogen) and then digested by *Eco*RI. The digested insert was extracted from agarose gel using Concert Kit (GibcoBRL). This cDNA was then labeled as a probe with [α-^{32}P]dCTP using MegaPrime DNA labeling system (Amersham Pharmacia Biotech). Ten micrograms of total RNA from 6-week-old Wt and Tg cardiac muscle were separated on 0.7% agarose gels containing 7% formaldehyde and blotted onto Hybond-N+ (Amersham Pharmacia Biotech). Hybridization was performed at 42°C for 12–24 h and autoradiography was performed on a Fuji imaging plate (Fuji Film). Signal intensity of transcripts was measured by BAS2000 Image Analyzer (Fuji Film). Using the same method, we hybridized northern blots with RT–PCR generated and labeled fragments of ANP cDNA, BNP cDNA, eNOS cDNA, nNOS cDNA, iNOS cDNA and internal control GAPDH cDNA.

Immunoblot analysis

Six-week-old Wt or Tg mouse cardiac muscle was homogenized in 10 vols (w/v) of a buffer containing 50 mM Tris–HCl (pH 7.4), 100 mM NaCl, 1 mM ethylenediaminetetraacetic acid (EDTA), 5 mM β-mercaptoethanol, 0.1 mM phenylmethylsulphonyl fluoride (PMSF) and 1 mM benzamidine. These crude extracts were denatured and size fractionated by SDS–PAGE (3–12%) and then transferred to a polyvinylidine difluoride (PVDF) membrane. The membrane was blocked using 5% milk in phosphate-buffered saline (PBS) and incubated with rabbit polyclonal antibody against caveolin-3 (Transduction Laboratories, C38330), raised against synthetic peptide corresponding to the amino terminus of caveolin-3 of rat and mouse origin, a monoclonal antibody against β-dystoglycan (Novo Castra), a rabbit polyclonal antibody against eNOS (Santa Cruz Biotechnology), a rabbit polyclonal antibody against nNOS (Santa Cruz Biotechnology) and a rabbit polyclonal antibody against iNOS (Transduction Laboratories) overnight at room temperature. After washing with 5% milk in PBS, the blots were incubated with horseradish peroxidase-conjugated anti-rabbit or anti-mouse IgG antibody (Amersham Pharmacia Biotech). Immunoreactive bands were visualized with ECL (Amersham Pharmacia Biotech).

Immunohistochemical analysis

Unfixed cardiac muscle samples were snap frozen in liquid nitrogen-cooled isopentane, sectioned on a cryostat (10 μm), and melted directly onto glass slides. Sections were then post-fixed in 4% freshly depolymerized paraformaldehyde in PBS for 15–30 min at 4°C. After blocking with 3% BSA in PBS, sections were immunostained with a goat polyclonal antibody against caveolin-3 (Santa Cruz Biotechnology, *sc-7665*), recognizing the epitope mapped at the amino terminus of caveolin-3 of mouse origin, a rabbit polyclonal antibody against caveolin-1 (Santa Cruz Biotechnology), a goat polyclonal antibody against dystrophin (Santa Cruz Biotechnology), and a rabbit polyclonal antibody against eNOS (Santa Cruz Biotechnology) for 1 h at room temperature. After extensive washing with PBS, sections were incubated with FITC-conjugated or Cy3-conjugated secondary antibody. Rabbit and goat polyclonal antibodies against caveolin-3 used in immunoblot and immunohistochemical analyses can recognize both mutant and wild type forms of caveolin-3.

Transthoracic echocardiogram

Transthoracic echocardiography was performed on 24-week-old Tg mice and Wt littermates ($n = 7$) under light anesthesia using intraperitoneal pentobarbital as described previously (30).

NOS assay

Total NOS activity was measured by monitoring the conversion of L-[^{3}H]arginine to L-[^{3}H]citrulline, as previously described (18,31–33). Briefly, freshly prepared cardiac muscle from 6-week-old Tg mice and Wt littermates ($n = 8$) was homogenized in 10 vols (w/v) of a buffer containing 50 mM Tris–HCl (pH 7.4), 100 mM NaCl, 0.5 mM EDTA, 0.5 mM EGTA, 1 mM DTT, 0.1 mM PMSF, and 1 μM leupeptin. Aliquots from crude homogenates were quickly assayed in 100 μl reactions containing 100 000 cpm (40 Ci/mmol) of L-[^{3}H]arginine, 1 mM NADPH, 50 mM Tris–HCl (pH 7.4), 100 mM NaCl, 1.2 mM $CaCl_2$, 10 μg/ml calmodulin, 1 mM DTT and 10 μM each of tetrahydrobiopterin, FAD and FMN. After an incubation of 10 min at 37°C, assays were terminated with 900 μl of ice cold H_2O. After brief sonication, samples were applied to 2 ml of Dowex AG 50W-X8 (Na^+ form) column. L-[^{3}H]citrulline was quantified using 1 ml flow-through by liquid scintillation spectroscopy. The combined activity of eNOS plus iNOS was also measured in the same reaction buffer containing specific inhibitor of nNOS (0.1 μM N^{ω}-propyl-L-arginine) (TOCRIS) (34,35). iNOS activity was also measured in the presence of 1.5 mM EDTA and 1.5 mM EGTA, which replaced Ca^{2+} ion in the reaction buffer. The above three assays were performed simultaneously. Then, nNOS activity was calculated by subtraction of the combined activity of eNOS and iNOS from total NOS activity. eNOS activity was calculated by subtraction of iNOS activity from the combined activity of eNOS and iNOS. Data are expressed as mean ± SD. Statistical significance was determined using Welch's *t*-test ($P < 0.05$).

ACKNOWLEDGEMENTS

We thank Drs Tsutomu Ogura, Yukiko Kurashima (Investigative Treatment Division, National Cancer Center Research Institute East) and Hiroshi Shima (Division of Biochemical Oncology and Immunology, Institute for Genetic Medicine, Hokkaido University) for their appropriate advice about the NOS assay method. We also thank Kenzo Uehira (Electron Microscopy Center, Kawasaki Medical School) and Megumu

Kita (Laboratory Animal Center, Kawasaki Medical School) for their technical assistance. This work was supported by Research Grant (14B-4) for Nervous and Mental Disorders from the Ministry of Health, Labour and Welfare, Research Grant (15130301) for Research on Psychiatric and Neurological Diseases and Mental Health from the Ministry of Health, Labour and Welfare, Research Grant (14370212) from the Ministry of Education, Culture, Sports, Science and Technology, and Research Project Grants (no. 13-105, 14-117, 14-505, 14604 and 14-208) from Kawasaki Medical School.

REFERENCES

1. Razani, B., Schlegel, A. and Lisanti, M.P. (2000) Caveolin proteins in signaling, oncogenic transformation and muscular dystrophy. *J. Cell Sci.*, **113**, 2103–2109.
2. Monier, S., Parton, R.G., Vogel, F., Behlke, J., Henske, A. and Kurzchalia, T.V. (1995) VIP21-caveolin, a membrane protein constituent of the caveolar coat, oligomerizes *in vivo* and *in vitro*. *Mol. Biol. Cell*, **6**, 911–927.
3. Couet, J., Li, S., Okamoto, T., Ikezu, T. and Lisanti, M.P. (1997) Identification of peptide and protein ligands for the caveolin-scaffolding domain. Implications for the interaction of caveolin with caveolae-associated proteins. *J. Biol. Chem.*, **272**, 6525–6533.
4. Galbiati, F., Razani, B. and Lisanti, M.P. (2001) Emerging themes in lipid rafts and caveolae. *Cell*, **106**, 403–411.
5. Feron, O., Belhassen, L., Kobzik, L., Smith, T.W., Kelly, R.A. and Michel, T. (1996) Endothelial nitric oxide synthase targeting to caveolae. Specific interactions with caveolin isoforms in cardiac myocytes and endothelial cells. *J. Biol. Chem.*, **271**, 22810–22814.
6. Kobzik, L., Reid, M.B., Bredt, D.S. and Stamler, J.S. (1994) Nitric oxide in skeletal muscle. *Nature*, **372**, 546–548.
7. Venema, V.J., Ju, H., Zou, R. and Venema, R.C. (1997) Interaction of neuronal nitric-oxide synthase with caveolin-3 in skeletal muscle. Identification of a novel caveolin scaffolding/inhibitory domain. *J. Biol. Chem.*, **272**, 28187–28190.
8. Garcia-Cardena, G., Martasek, P., Masters, B.S., Skidd, P.M., Couet, J., Li, S., Lisanti, M.P. and Sessa, W.C. (1997) Dissecting the interaction between nitric oxide synthase (NOS) and caveolin. Functional significance of the NOS caveolin binding domain *in vivo*. *J. Biol. Chem.*, **272**, 25437–25440.
9. Minetti, C., Sotgia, F., Bruno, C., Scartezzini, P., Broda, P., Bado, M., Masetti, E., Mazzocco, M., Egeo, A., Donati, M.A. *et al.* (1998) Mutations in the caveolin-3 gene cause autosomal dominant limb-girdle muscular dystrophy. *Nat. Genet.*, **18**, 365–368.
10. Betz, R.C., Schoser, B.G., Kasper, D., Ricker, K., Ramirez, A., Stein, V., Torbergsen, T., Lee, Y.A., Nothen, M.M., Wienker, T.F. *et al.* (2001) Mutations in CAV3 cause mechanical hyperirritability of skeletal muscle in rippling muscle disease. *Nat. Genet.*, **28**, 218–219.
11. Sunada, Y., Ohi, H., Hase, A., Ohi, H., Hosono, T., Arata, S., Higuchi, S., Matsumura, K. and Shimizu, T. (2001) Transgenic mice expressing mutant caveolin-3 show severe myopathy associated with increased nNOS activity. *Hum. Mol. Genet.*, **10**, 173–178.
12. Fujita, T., Toya, Y., Iwatsubo, K., Onda, T., Kimura, K., Umemura, S. and Ishikawa, Y. (2001) Accumulation of molecules involved in alpha1-adrenergic signal within caveolae: caveolin expression and the development of cardiac hypertrophy. *Cardiovasc. Res.*, **51**, 709–716.
13. Winlaw, D.S., Smythe, G.A., Keogh, A.M., Schyvens, C.G., Spratt, P.M. and Macdonald, P.S. (1994) Increased nitric oxide production in heart failure. *Lancet*, **344**, 373–374.
14. Stein, B., Eschenhagen, T., Rudiger, J., Scholz, H., Forstermann, U. and Gath, I. (1998) Increased expression of constitutive nitric oxide synthase III, but not inducible nitric oxide synthase II, in human heart failure. *J. Am. Coll. Cardiol.*, **32**, 1179–1186.
15. Barouch, L.A., Harrison, R.W., Skaf, M.W., Rosas, G.O., Cappola, T.P., Kobeissi, Z.A., Hobai, I.A., Lemmon, C.A., Burnett, A.L., O'Rourke, B. *et al.* (2002) Nitric oxide regulates the heart by spatial confinement of nitric oxide synthase isoforms. *Nature*, **416**, 337–341.
16. Balligand, J.L., Kelly, R.A., Marsden, P.A., Smith, T.W. and Michel, T. (1993) Control of cardiac muscle cell function by an endogenous nitric oxide signaling system. *Proc. Natl Acad. Sci. USA*, **90**, 347–351.
17. Klabunde, R.E., Kimber, N.D., Kuk, J.E., Helgren, M.C. and Forstermann, U. (1992) N^G-methyl-L-arginine decreases contractility, cGMP and cAMP in isoproterenol-stimulated rat hearts *in vitro*. *Eur. J. Pharmac.*, **223**, 1–7.
18. Balligand, J.L., Kobzik, L., Han, X., Kaye, D.M., Belhassen, L., O'Hara, D.S., Kelly, R.A., Smith, T.W. and Michel, T. (1995) Nitric oxide-dependent parasympathetic signaling is due to activation of constitutive endothelial (type III) nitric oxide synthase in cardiac myocytes. *J. Biol. Chem.*, **270**, 14582–14586.
19. Hare, J.M., Lofthouse, R.A., Juang, G.J., Colman, L., Ricker, K.M., Kim, B., Senzaki, H., Cao, S., Tunin, R.S. and Kass, D.A. (2000) Contribution of caveolin protein abundance to augmented nitric oxide signaling in conscious dogs with pacing-induced heart failure. *Circul. Res.*, **86**, 1085–1092.
20. Hare, J.M., Givertz, M.M., Creager, M.A. and Colucci, W.S. (1998) Increased sensitivity to nitric oxide synthase inhibition in patients with heart failure: potentiation of β-adrenergic inotropic responsiveness. *Circulation*, **97**, 161–166.
21. Vila-Petroff, M.G., Kim, S.H., Pepe, S., Dessy, C., Marban, E., Balligand, J.L. and Sollott, S.J. (2001) Endogenous nitric oxide mechanisms mediate the stretch dependence of Ca^{2+} release in cardiomyocytes. *Nat. Cell. Biol.*, **3**, 867–873.
22. Xu, K.Y., Huso, D.L., Dawson, T.M., Bredt, D.S. and Becker, L.C. (1999) Nitric oxide synthase in cardiac sarcoplasmic reticulum. *Proc. Natl Acad. Sci. USA*, **96**, 657–662.
23. Xu, L., Eu, J.P., Meissner, G. and Stamler, J.S. (1998) Activation of the cardiac calcium release channel (ryanodine receptor) by poly-*S*-nitrosylation. *Science*, **279**, 234–237.
24. Brunner, F., Andrew, P., Wolkart, G., Zechner, R. and Mayer, B. (2001) Myocardial contractile function and heart rate in mice with myocyte-specific overexpression of endothelial nitric oxide synthase. *Circulation*, **104**, 3097–3102.
25. Mery, P.F., Pavoine, C., Belhassen, L., Pecker, F. and Fischmeister, R. (1993) Nitric oxide regulates cardiac Ca^{2+} current. Involvement of cGMP-inhibited and cGMP-stimulated phosphodiesterases through guanylyl cyclase activation. *J. Biol. Chem.*, **268**, 26286–26295.
26. Vila-Petroff, M.G., Younes, A., Egan, J., Lakatta, E.G. and Sollott, S.J. (1999) Activation of distinct cAMP-dependent and cGMP-dependent pathways by nitric oxide in cardiac myocytes. *Circul. Res.*, **84**, 1020–1031.
27. Shah, A.M., Spurgeon, H.A., Sollott, S.J., Talo, A. and Lakatta, E.G. (1994) 8-bromo-cGMP reduces the myofilament response to Ca^{2+} in intact cardiac myocytes. *Circul. Res.*, **74**, 970–978.
28. Woodman, S.E., Park, D.S., Cohen, A.W., Cheung, M.W., Chandra, M., Shirani, J., Tang, B., Jelicks, L.A., Kitsis, R.N., Christ, G.J. *et al.* (2002) Caveolin-3 knock-out mice develop a progressive cardiomyopathy and show hyperactivation of the p42/44 MAPK cascade. *J. Biol. Chem.*, **277**, 38988–38997.
29. Ricker, K., Moxley, R.T. and Rohkamm, R. (1989) Rippling muscle disease. *Arch. Neurol.*, **46**, 405–408.
30. Toko, H., Oka, T., Zou, Y., Sakamoto, M., Mizukami, M., Sano, M., Yamamoto, R., Sugaya, T. and Komuro, I. (2002) Angiotensin II type 1a receptor mediates doxorubicin-induced cardiomyopathy. *Hypertens. Res.*, **25**, 597–603.
31. Bredt, D.S. and Snyder, S.H. (1990) Isolation of nitric oxide synthase, a calmodulin-requiring enzyme. *Proc. Natl Acad. Sci. USA*, **87**, 682–685.
32. Shulz, R., Nava, E. and Moncada, S. (1992) Induction and potential biological relevance of a Ca^{2+}-independent nitric oxide synthase in the myocardium. *Br. J. Pharmac.*, **105**, 575–580.
33. Bia, B.L., Cassidy, P.J., Young, M.E., Rafael, J.A., Leighton, B., Davies, K.E., Radda, G.K. and Clark, K. (1999) Decreased myocardial nNOS, increased iNOS and abnormal ECGs in mouse models of Duchenne muscular dystrophy. *J. Mol. Cell. Cardiol.*, **31**, 1857–1862.
34. Zhang, H.Q., Fast, W., Marletta, M.A., Martasek, P. and Silverman, R.B. (1997) Potent and selective inhibition of neuronal nitric oxide synthase by N^{ω}-propyl-L-arginine. *J. Med. Chem.*, **40**, 3869–3870.
35. Kakoki, M., Zou, A.-P. and Mattson, D.L. (2001) The influence of nitric oxide synthase 1 on blood flow and interstitial nitric oxide in the kidney. *Am. J. Physiol. Regul. Integr. Comp. Physiol.*, **281**, R91–R97.

THE JOURNAL OF BIOLOGICAL CHEMISTRY
Vol. 279, No. 12, Issue of March 19, pp. 11384–11391, 2004
Printed in U.S.A.
© 2004 by The American Society for Biochemistry and Molecular Biology, Inc.

Adult Cardiac Sca-1-positive Cells Differentiate into Beating Cardiomyocytes*[S]

Received for publication, October 1, 2003, and in revised form, December 16, 2003
Published, JBC Papers in Press, December 31, 2003, DOI 10.1074/jbc.M310822200

Katsuhisa Matsuura‡§, Toshio Nagai‡, Nobuhiro Nishigaki‡¶, Tomomi Oyama‡, Junichiro Nishi‡, Hiroshi Wada‡, Masanori Sano‡, Haruhiro Toko‡, Hiroshi Akazawa‡, Toshiaki Sato‖, Haruaki Nakaya‖, Hiroshi Kasanuki§, and Issei Komuro‡**

From the ‡Department of Cardiovascular Science and Medicine, Chiba University Graduate School of Medicine, Chiba 260-8670, Japan, the §Department of Cardiology, The Heart Institute of Japan, Tokyo Women's Medical University, Tokyo 162-0054, Japan, the ¶Takeda Chemical Industries, LTD, Osaka 540-8645, Japan, and the ‖Department of Pharmacology, Chiba University Graduate School of Medicine, Chiba 260-8670, Japan

Although somatic stem cells have been reported to exist in various adult organs, there have been few reports concerning stem cells in the heart. We here demonstrate that Sca-1-positive (Sca-1+) cells in adult hearts have some of the features of stem cells. Sca-1+ cells were isolated from adult murine hearts by a magnetic cell sorting system and cultured on gelatin-coated dishes. A fraction of Sca-1+ cells stuck to the culture dish and proliferated slowly. When treated with oxytocin, Sca-1+ cells expressed genes of cardiac transcription factors and contractile proteins and showed sarcomeric structure and spontaneous beating. Isoproterenol treatment increased the beating rate, which was accompanied by the intracellular Ca^{2+} transients. The cardiac Sca-1+ cells expressed oxytocin receptor mRNA, and the expression was up-regulated after oxytocin treatment. Some of the Sca-1+ cells expressed alkaline phosphatase after osteogenic induction and were stained with Oil-Red O after adipogenic induction. These results suggest that Sca-1+ cells in the adult murine heart have potential as stem cells and may contribute to the regeneration of injured hearts.

The heart has long been thought to adapt to increased work and loss of cardiomyocytes by the cellular hypertrophy of residual cardiomyocytes, but not by the proliferation of mature cardiomyocytes or the differentiation of undifferentiated cells. However, recent reports have suggested that adult cardiomyocytes can proliferate under certain pathologic conditions and that there are cells expressing stem cell markers in the adult heart (1–4). It has been reported that Sca-1- and c-kit-positive (+) cells exist in the adult heart (5) and that adult murine hearts contain potential stem cells; side population (SP)[1] cells (6, 7). However, it remains to be clarified whether these cells have the characteristics of stem cells such as abilities of self-renewal and differentiation into various types of cells including mature cardiomyocytes.

Sca-1 is a member of the Ly-6 family and has first reported as one of the cell surface markers of hematopoietic stem cells (8). Recently many reports have demonstrated that multipotential stem cells derived from bone marrow and skeletal muscle express Sca-1. Okumoto *et al.* (9) have reported that Sca-1+ cells from bone marrow differentiate into hepatocyte when treated with hepatic growth factor. Gojo *et al.* (10) have reported that adult mesenchymal stem cells from bone marrow abundantly express Sca-1 and differentiate into cardiomyocyte *in vivo*. Qu-Petersen *et al.* (11) have shown that skeletal muscle-derived stem cells, which highly express Sca-1, contribute to the regeneration of the skeletal muscle in a mouse model of Duchenne muscle dystrophy. They also demonstrated that the skeletal muscle-derived stem cells were able to differentiate into neural cells and endothelial cells. Asakura *et al.* (12) have reported that ~90% of SP cells in skeletal muscle express Sca-1. It has been reported that skeletal muscle-derived Sca-1+ and CD34+ cells restore dystrophin in mdx mice (13) and that CD34+ and CD45− cells in the interstitial spaces of skeletal muscle, which highly express Sca-1, differentiate into adipocytes, endothelial, and myogenic cells (14). These findings suggest that Sca-1 might be important evidence for somatic stem cells.

Currently little is known about the humoral or growth factors that induce cardiomyogenic differentiation. It has been shown that ectopic application of bone morphological protein (BMP) 2 and 4 elicits cardiogenic responses in the chick *in vivo* system (15), and fibroblast growth factor (FGF) 2 and 4, combined with BMP-2 or BMP-4 can induce cardiogenesis in chick non-precardiac mesoderm (16). The non-canonical Wnt/c-Jun-N-terminal kinase pathways have been reported to be essential for cardiac induction in frog and chick embryo systems (17, 18). These factors are prerequisites for early cardiac differentiation but are not sufficient for accomplishing differentiation into mature beating cardiomyocytes. Recently Paquin *et al.* (19) have reported that oxytocin induces differentiation of P19 embryonic carcinoma cells to beating cardiomyocytes. In support of the role of oxytocin in cardiac development, the oxytocin receptor is increased at the protein level in the murine heart from day 7 of gestation, when cardiac differentiation starts

* This study was supported by a grant-in-aid for Scientific Research, Developmental Scientific Research, and Scientific Research on Priority Areas from the Ministry of Education, Science, Sports, and Culture, Takeda Medical Research Foundation, Uehara Memorial Foundation, grant-in-aid of The Japan Medical Association, The Kato Memorial Trust for Nambyo Research, Takeda Science Foundation, and a Japan Heart Foundation Research Grant. The costs of publication of this article were defrayed in part by the payment of page charges. This article must therefore be hereby marked "*advertisement*" in accordance with 18 U.S.C. Section 1734 solely to indicate this fact.

[S] The on-line version of this article (available at http://www.jbc.org) contains Supplementary Data.

** To whom correspondence should be addressed: Dept. of Cardiovascular Science and Medicine, Chiba University Graduate School of Medicine, 1-8-1 Inohana, Chuo-ku, Chiba 260-8670 Japan. Tel.: 81-43-226-2097; Fax: 81-43-226-2096; E-mail: komuro-tky@umin.ac.jp.

[1] The abbreviations used are: SP, side population; PE, phycoerythrin; PBS, phosphate-buffered saline; FBS, fetal bovine serum; MHC, myosin heavy chain; MLC, myosin light chain; MACS, Magnetic Cell Sorting; ALP, alkaline phosphatase; MEF, muscle enhancer factor.

This paper is available on line at http://www.jbc.org

TABLE I
PCR primers and PCR conditions

Primer	Product size	Annealing temperature
	bp	°C
α-MHC		
5′-GGAAGAGTGAGCGGCCATCAAGG-3′	302	65
5′-CTGCTGGAGAGGTTATTCCTCG-3′		
β-MHC		
5′-GCCAACACCAACCTGTCCAAGTTC-3′	205	66
5′-TGCAAAGGCTCCAGGTCTGAGGGC-3′		
MLC-2a		
5′-CAGACCTGAAGGAGACCT-3′	286	54
5′-GTCAGCGTAAACAGTTGC-3′		
MLC-2v		
5′-GCCAAGAAGCGGATAGAAGG-3′	499	55
5′-CTGTGGTTCAGGGCTCAGTC-3′		
Cardiac α-actin		
5′-CTGAGATGTCTCTCTCTCTTAG-3′	99	60
5′-ACAATGACTGATGAGAGATG-3′		
Csx/Nkx-2.5		
5′-CAGTGGAGCTGGACAAAGCC-3′	216	55
5′-TAGCGACGGTTCTGGAATTT-3′		
GATA4		
5′-CTGTCATCTCACTATGGGCA-3′	275	60
5′-CCAAGTCCGAGCAGGAATTT-3′		
MEF-2C		
5′-GGCCATGGTACACCGAGTACAACGAGC-3′	401	62
5′-GGGGATCCCTGTGTTACCTGCACTTGG-3′		
Oxytocin receptor		
5′-AAGATGACCTTCATCATTGTTC-3′	303	61
5′-CGACTCAGGACGAAGGTGGAGGA-3′		
ALP		
5′-TTGAAACTCCAAAAGCTCAACACCA-3′	450	62
5′-TCTCGTTATCCGAGTACCAGTCCC-3′		
Osteocalcin		
5′-CCGGGAGCAGTGTGAGCTTA-3′	92	62
5′-TAGATGCGTTTGTAGGCGGTC-3′		
β-Actin		
5′-GGACCTGGCTGGCCGGGACC-3′	583	60
5′-GCGGTGCACGATGGAGGGGC-3′		

(20). Although the precise mechanism of the effect of oxytocin is not clear, oxytocin may play an important role in the differentiation into cardiomyocytes from primitive cells including adult somatic stem cells. Here, we first report that a novel population from Sca-1+ cells derived from the adult murine heart proliferates and differentiates into beating cardiomyocytes with oxytocin treatment.

EXPERIMENTAL PROCEDURES

Animals and Reagents—Wild mice (C57Bl/6) were purchased from Takasugi Experimental Animals Supply, Co, LTD, Japan. All protocols were approved by the Institutional Animal Care and Use Committee of Chiba University. Phycoerythrin (PE) -conjugated anti-Sca-1 (anti-Ly6A/E), anti-c-kit (anti-CD117) antibodies were purchased from eBioscience (San Diego, CA). PE-conjugated anti-CD34, anti-CD45, and biotin-conjugated anti-Sca-1 antibodies were purchased from BD Pharmingen (San Diego, CA). The following antibodies were used for immunostaining: mouse monoclonal anti-cardiac troponin T (RV-C2, DSMZ-Deutsche Sammlung von Mikroorganismen und Zellkulturen GmbH, Germany), rabbit polyclonal anti-atrial natriuretic factor-1 (ANF) (Peninsula Laboratories, San Carlos. CA), goat polyclonal anti-GATA4 (Santa Cruz Biotechnology, Santa Cruz, CA), mouse monoclonal anti-myosin light chain-2v (MLC-2v) (BioCytex, France), mouse monoclonal anti-tropomyosin (Sigma Aldrich), mouse monoclonal anti-sarcomeric myosin heavy chain (MF-20) (American Type Culture Collection), rabbit polyclonal anti-connexin 43 (Zymed Laboratories, South San Francisco, CA). Fluorescent secondary antibodies were purchased from Jackson ImmunoResearch Laboratory (Bar Harbor, ME). Other reagents that are not specified were obtained from Sigma-Aldrich.

Isolation and Culture of Sca-1+ Cells from the Adult Murine Heart—A heart of adult C57Bl/6 mouse (10–12 weeks old) was enzymatically dissociated into a single cell suspension as described previously (21). Enrichment of Sca-1+ cells was achieved by sorting using the Magnetic Cell Sorting (MACS) system (Miltenyl Biotec, Sunnyvale, CA). Whole primary cell suspension was incubated with PE-conjugated anti-Sca-1 antibody for 10 min on ice, washed in PBS supplemented with 3% FBS, incubated with anti-PE micro beads for 15 min at 4 °C, and washed with PBS supplemented with 3% FBS. The samples were passed through a MACS column set up in a Miltenyl magnet and the Sca-1+ cells were eluted from the column by washing with PBS supplemented with 3% FBS. To increase the purity of the Sca-1+ cells, magnetic sorting was performed one more time. The Sca-1+ cells were cultured on 1% gelatin-coated dishes with Iscove's Modified Dulbecco's Medium (IMDM) supplemented with 10% FBS, 100 μg/ml of penicillin, and 250 μg/ml of streptomycin at 37 °C in humid air with 5% CO_2. Twenty-four hours after seeding, the cells were treated with 10 μM 5′-azacytizine for the initial 72 h or 100 nM oxytocin (WAKO, Japan). After treatment, the medium was changed every 3 days.

Characterization of Cardiac Muscle-derived Stem Cells for Flow Cytometric Analysis—Sca-1+ cells were isolated by the MACS system with biotin-conjugated anti-Sca-1 antibody and anti-biotin micro beads. Magnetic sorting was repeated twice, and the cells were incubated with PE-conjugated anti-CD45 antibody, PE-conjugated anti-CD34 antibody, and PE-conjugated anti-c-kit antibody, respectively for 10 min on ice and washed with PBS supplemented with 3% FBS. The percentages of CD45+, CD34+, and c-kit+ cells were analyzed by the EPICS ALTRA flow cytometer using EXPO32 software (Beckman Coulter, Miami, FL).

RNA Extraction and Reverse Transcriptase-PCR—Total RNA was extracted from the adult murine heart, liver, and Sca-1+ cells by RNA-bee reagent (TEL-TEST, Friendswood, TX). Reverse transcriptase (RT)-PCR of genes of cardiac transcription factors, including Csx/Nkx-2.5 (22), GATA4 (23), muscle enhancer factor-2C (MEF-2C) (24), and cardiac structural proteins, including α- and β-myosin heavy chain (MHC) (25), myosin light chain-2a (MLC-2a), MLC-2v (26), cardiac α-actin (27), and oxytocin receptor (19), alkaline phosphatase (28), osteocalcin (29) were performed using 0.1 μg of total RNA. β-actin (30) was used as an internal control. The primers used in this study and PCR conditions are described in Table I. The PCR products were size-fractionated by 2% agarose gel electrophoresis.

Immunocytochemistry—Cells were fixed with 4% paraformaldehyde for 15 min at room temperature. After preblocking with PBS containing 2% donkey serum, 2% bovine serum albumin and 0.2% Nonidet P-40 for

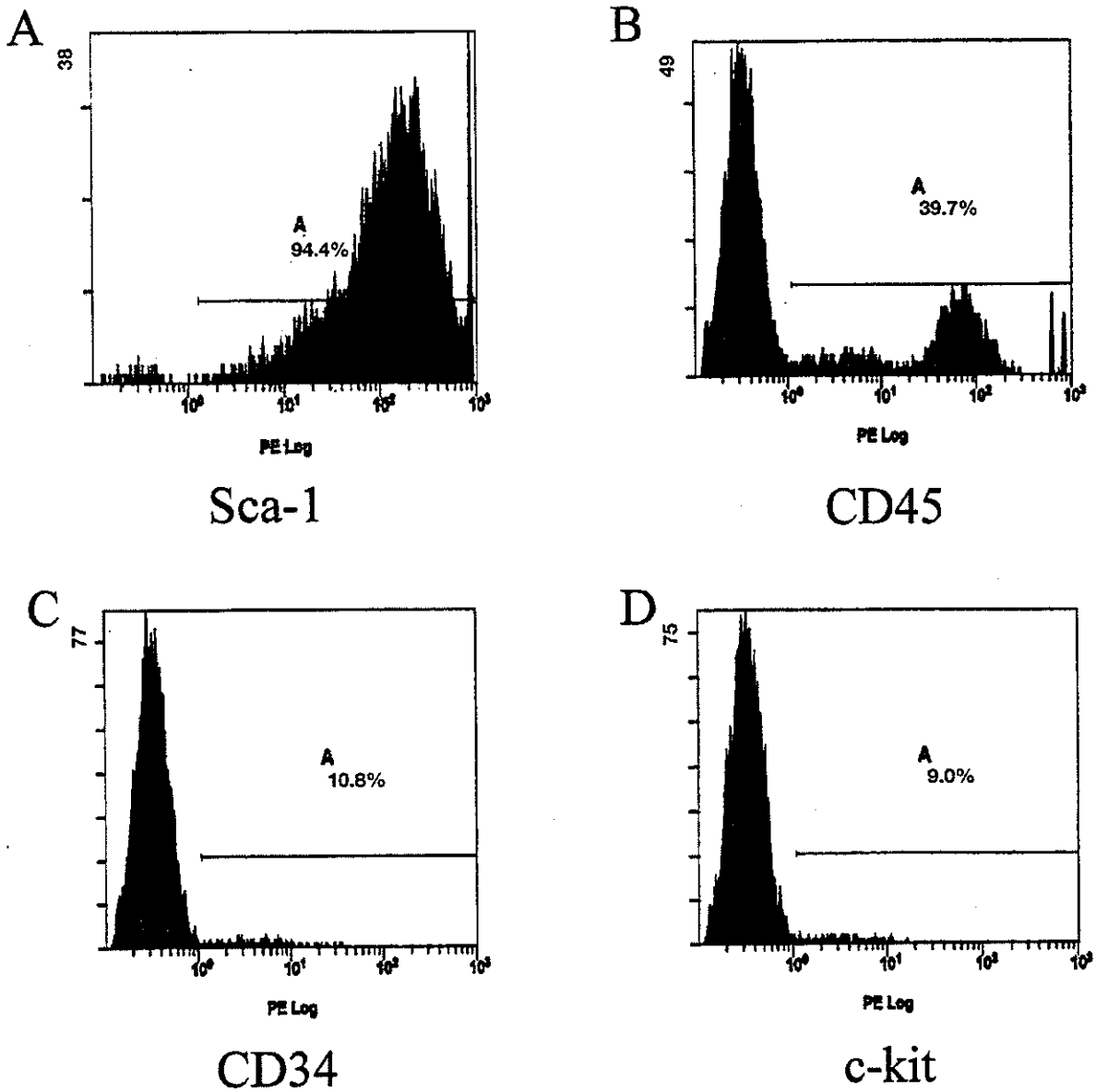

FIG. 1. **Flow cytometric analysis of Sca-1+ cells.** Sca-1+ cells were enriched by the MACS system with PE-conjugated anti-Sca-1 antibody and anti-PE micro beads, and after sorting twice, ~90% of the cells expressed Sca-1 (*A*). Sca-1+ cells were stained with PE-conjugated anti-CD45 antibody, anti-CD34 antibody, and anti-c-kit antibody. In enriched Sca-1+ cells, ~40% of the cells expressed CD45 (*B*), ~10% of the cells expressed CD34 (*C*), and c-kit (*D*).

30 min, primary antibodies in PBS containing 2% donkey serum, 2% bovine serum albumin and 0.1% Nonidet P-40 were applied overnight in 4 °C. Subsequently cells were washed three times in PBS, and then fluorescein isothiocyanate- or Cy5-conjugated secondary antibodies were applied to visualize expression of specific proteins. Nuclear staining was performed with TO-PRO-3 (Molecular Probes, Eugene, OR). Images of cells were taken by laser confocal microscopy (Radiance2000, Bio-Rad, Hercules, CA).

Phase Contrast Live Imaging—Live images were taken by a Zeiss inverted microscope (Carl Zeiss, Jena, Germany) equipped with phase-contrast objectives and an AxioCam camera. Live image of beating cells were obtained by a chilled CCD camera (Hamamatsu) using I-O DATA Videorecorder software.

Measurement of Intracellular Ca^{2+} Concentration—Intracellular Ca^{2+} concentration ($[Ca^{2+}]_i$) in beating cells derived from cardiac Sca-1+ cells was measured as previously described (31). The beating cells on gelatin-coated glass coverslips were incubated in HEPES (loading) solution containing 1 μM fluo 3-acetoxymethyl ester (fluo 3-AM; Molecular Probes) at 36 °C in the dark for 30 min. The loading solution was prepared by diluting a 100 μM fluo 3 stock solution, which contained 0.45% Pluronic F127 (Molecular Probes), 10% dimethyl sulfoxide, and 90% FBS. HEPES solution consisted of (in mM) 126 NaCl, 4.4 KCl, 1.0 $MgCl_2$, 1.08 $CaCl_2$, 24 HEPES, 13 NaOH, 11 glucose, and 0.5 probenecid (pH 7.4). The coverslips were washed twice with dye-free HEPES solution and placed in a flow-through chamber on the microscope. Fluo 3-loaded beating cells were excited by 480-nm light and emitted fluorescence was recorded at 530 nm by a photomultiplier tube (AIM-10, InterMedical, Co, Japan) and digitized (PowerLab 2/20, AD-instruments, Castle Hill, Australia). Curve fits were performed with Origin 7J software (MicroCal Software, Northampton, MA). The intensity of the fluorescence at 530 nm increased with an increase in $[Ca^{2+}]_i$.

Estimation of Pluripotency—Osteogenic differentiation of Sca-1+ cells from the adult murine heart was induced in IMDM supplemented with 10% FBS, 50 μM ascorbic acid 2-phosphate, 0.1 μM dexamethasone, and 10

mM β-glycerophosphate as described previously (32). For detection of osteocytes, alkaline phosphatase staining (leukocyte alkaline phosphatase assay kit, Sigma-Aldrich) was used. Adipogenic differentiation was induced as described previously (28). Briefly the cells were cultured with Dulbecco's Modified Eagle's Medium (DMEM) supplemented with 5% horse serum with MDI-I mixture; 0.5 mM methyl-isobutylxanthine, 1 μM dexamethasone, 100 mM indomethacin, and 10 μg/ml insulin for 2 days and then cultured with Dulbecco's modified Eagle's medium supplemented with 5% horse serum and 10 μg/ml of insulin for 1 day. Treatment with MDI-I followed by insulin was repeated four times. For detection of accumulated oil droplets, Oil-Red O staining was performed followed by nuclear hematoxylin counterstaining.

Statistical Analysis—Values are presented as mean ± S.E. The significance of differences among mean values was determined by analysis of variance. The accepted level of significance was $p < 0.05$.

RESULTS

Cell Surface Antigens of Sca-1+ Cells Derived from the Adult Murine Heart—Flow cytometric analysis revealed that Sca-1+ cells were enriched to over 90% when adult murine cardiac cells were sorted twice with the MACS system using PE-conjugated anti-Sca-1 antibody and anti-PE micro beads (Fig. 1*A*). The number of purified Sca-1+ cells was ~1×10^4 cells. Limana *et al.* (33) have estimated the number of cardiomyocytes in an adult murine heart as ~3×10^6. Therefore the percentage of cardiac Sca-1+ cells was ~0.3% of the total number of cardiomyocytes. Next we examined other cell surface antigens such as CD45, CD34, and c-kit in Sca-1+ cells. After repeated magnetic sorting with biotin-conjugated anti-Sca-1 antibody and anti-biotin micro beads, enriched Sca-1+ cells were incubated with PE-conjugated anti-CD45, CD34 and c-kit antibodies and analyzed by flow cytometry. In enriched Sca-1+ cells, ~40% of the cells expressed CD45 (Fig. 1*B*), and ~10% of the cells expressed CD34 (Fig. 1*C*) and c-kit (Fig. 1*D*).

Sca-1+ Cells from the Adult Murine Heart Differentiate into Beating Cardiomyocytes—In order to induce differentiation into cardiomyocytes, Sca-1+ cells were treated with either 5′-azacytizine or oxytocin. When Sca-1+ cells were cultured with medium containing FBS, they showed various cell shapes, and spindle-like and elongated shapes were predominant (Fig. 2*A*). Two weeks after treatment with oxytocin, small round cells with prominent nucleus and little cytoplasm appeared (*arrowheads* in Fig. 2*B*). These round cells rapidly proliferated, formed clusters, and detached from the culture dish so that spindle-shaped cells were left. The cells were re-plated when reached to confluence. Four weeks after starting treatment with oxytocin, some spontaneously beating cells were recognized among spindle-shaped cells (*arrow* in Fig. 2, *C* and *D* and Supplemental Data). Spontaneous beating was observed at ~1% cells. On the other hand, cells after treatment with 5′-azacytizine or vehicles showed fibroblast-like morphology, and never exhibited round or spindle-shaped morphology, or spontaneous beating.

Next we examined the gene expression of cardiac transcription factors and cardiac structural proteins in Sca-1+ cells by RT-PCR. Before treatment with 5′-azacytizine or oxytocin, only Csx/Nkx-2.5 and GATA4 were slightly expressed (Fig. 3, *lane P*). Four weeks after treatment with 5′-azacytizine or oxytocin, all genes of cardiac transcription factors including Csx/Nkx-2.5, GATA4, and MEF-2C and structural proteins such as α- and β-MHC, MLC-2a, MLC-2v, and cardiac α-actin were expressed (Fig. 3, *lane A* for 5′-azacytizine and *lane OT* for oxytocin). Treatment with 100 nM oxytocin antagonist (OTA, [d(CH_2)$_5$-1,Tyr(Me)-2,Thr-4,Orn-8,Tyr-NH_2-9] vasotocin, Wako, Japan) completely inhibited oxytocin-induced expression of cardiac genes (Fig. 3, *lane OT+OTA*). Total RNA obtained from the adult murine heart and liver were used as positive and negative controls (Fig. 3, *lane H* for heart and *lane L* for liver). Loading of equal amounts of RNA was confirmed by expression of the β-actin gene. Cardiac gene expression was not observed in cells cultured with vehicle (Fig. 3, *lane V*).

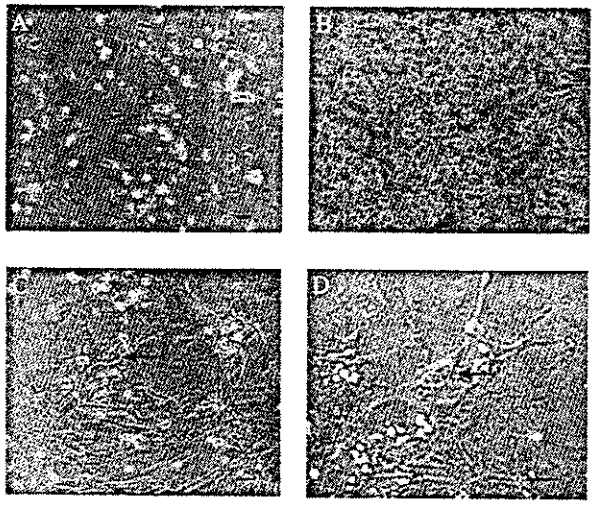

FIG. 2. **Phase contrast images of Sca-1+ cells before and after oxytocin treatment.** *A*, Sca-1+ cells before oxytocin treatment show small spindle-shaped morphology (0 weeks). *B*, two weeks after treatment with oxytocin, small round cells (*arrowheads*) have appeared. These round cells rapidly proliferated, formed clusters, and detached from the culture dish so that spindle-shaped cells were left. The cells were re-plated when reached to confluence. Four weeks after starting treatment with oxytocin, some spontaneously beating cells (*arrow* in *C* and *D*) were recognized among the spindle-shaped cells (*C*). *D*, magnified scale of the figure in *C*. *Bars*, 100 μM.

To examine the expression and localization of cardiac proteins, the Sca-1+ cells treated with oxytocin and 5′-azacytizine were stained with specific antibodies against cardiac proteins. The cells treated with oxytocin expressed GATA4 (Fig. 4*A*), ANF (Fig. 4*B*), and cardiac troponin T (Fig. 4, *A* and *B*). MLC-2v (Fig. 4*C*), sarcomeric myosin heavy chain (Fig. 4*D*), and tropomyosin (data not shown) were also expressed. Notably, staining of each contractile protein showed a fine striated pattern. Connexin 43 was expressed at the junction between two cardiac troponin T-expressing cells (Fig. 4*E*). These findings indicate that treatment with oxytocin induced differentiation of Sca-1+ cells, derived from the adult murine heart, into mature cardiomyocytes, which had well-organized structures and electrical junctions. After treatment with 5′-azacytizine, a fraction of cells expressed sarcomeric myosin heavy chain in fibrillar pattern (Fig. 4*F*), but not cardiac troponin T (data not shown). Next we sorted cardiac Sca-1+ cells on the basis of CD45 expression and cultured with oxytocin. Some of the Sca-1+/CD45− cells expressed sarcomeric myosin after oxytocin treatment, but none of the Sca-1+/CD45+ cells expressed myosin (data not shown), suggesting that Sca-1+ cells that can differentiate into cardiomyocytes are in CD45− population.

Cardiac contraction is regulated by beat to beat change in $[Ca^{2+}]_i$. To ascertain that the spontaneous beating of differentiated cardiac Sca-1+ cells depends on intracellular level of Ca^{2+}, we analyzed $[Ca^{2+}]_i$ transients of the beating cells. As shown in the *upper panel* of Fig. 5*A*, the spontaneous beating of differentiated Sca-1+ cells was accompanied with $[Ca^{2+}]_i$ transients. After treatment with 10^{-7} M isoproterenol for 5 min, the frequency of $[Ca^{2+}]_i$ transients was increased in comparison with control (Fig. 5*A*, *upper panel versus lower panel*). Next we examined the predominant subtype of β receptors, which mediates changes in beating rate. Differentiated cardiac Sca-1+ cells were treated with vehicle (PBS), propranolol, CGP20712A (β_1-selective blocker), or ICI118551 (β_2-selective blocker) for 30

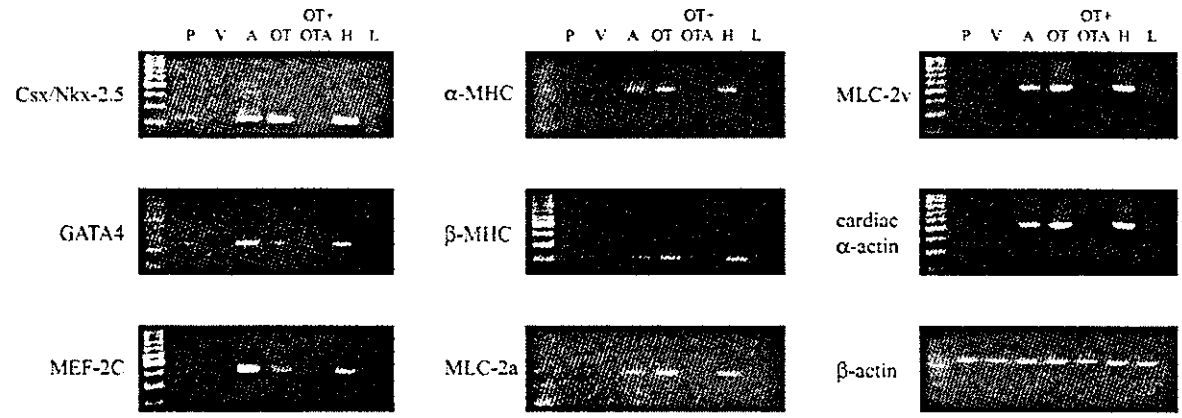

FIG. 3. **RT-PCR analysis of cardiac genes.** Sca-1+ cells after treatment with oxytocin (*lane OT*) or 5′-azacytizine (*lane A*) expressed Csx/Nkx-2.5, GATA4, MEF-2C, α-MHC, β-MHC, MLC-2a, MLC-2v, and cardiac α-actin. Although Sca-1+ cells before treatment (*lane P*) expressed Csx/Nkx-2.5 and GATA4 slightly, none of cells after treatment with vehicles (*lane V*) or oxytocin antagonist combined with oxytocin (*lane OT+OTA*) expressed any cardiac transcription factors. Heart (*lane H*) and liver (*lane L*) were used as positive and negative controls, respectively.

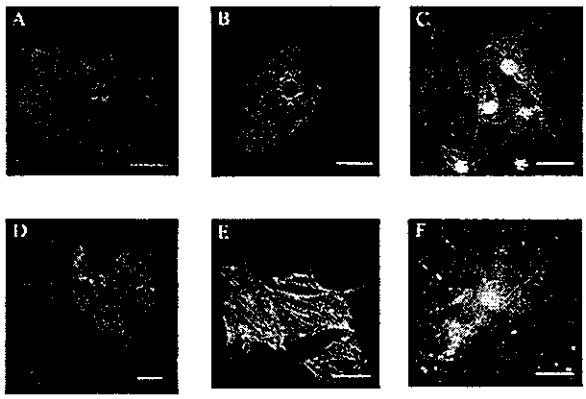

FIG. 4. **Immunocytochemical analysis of cardiac proteins.** *A–E*, cardiac differentiation of Sca-1+ cells after oxytocin treatment. Cells were double-stained using anti-GATA4 antibody (*A*, *green*), anti-ANF antibody (*B*, *green*), and anti-cardiac troponin T antibody (*A* and *B*, *blue*). Cells were stained with anti-MLC-2v (*C*, *green*) and anti-sarcomeric myosin heavy chain antibodies (*D*, *green*), and nuclei were stained with TO-PRO-3 (*C* and *D*, *blue*). Cells were double-stained using anti-cardiac troponin T antibody (*E*, *green*) and anti-connexin 43 antibody (*E*, *blue*). *F*, differentiation of Sca-1+ cells after 5′-azacytizine treatment. Cells were stained with anti-sarcomeric myosin heavy chain (*F*, *green*) and TO-PRO-3 (*F*, *blue*). *Bars*, 50 μm.

min and then stimulated with isoproterenol alone for 5 min. Isoproterenol significantly increased the beating rate of the control cells (control: 131.9 ± 5.6, $n = 10$ *versus* isoproterenol: 228.9 ± 7.3, $n = 10$, $p < 0.01$, Fig. 5*B*). The pretreatment with propranolol (average 196.4 ± 5.6, $n = 10$, $p < 0.05$ *versus* isoproterenol) and CGP20712A (average 188.9 ± 7.5, $n = 10$, $p < 0.05$ *versus* isoproterenol) reduced the increase in beating rate in response to isoproterenol significantly (Fig. 5*B*). ICI118551 had no effect on the isoproterenol-induced increase in beating rate.

Sca-1+ Cells from the Adult Murine Heart Express Oxytocin Receptor mRNA—To elucidate the role of oxytocin receptor in cardiomyogenesis of Sca-1+ cells, we examined the expression of oxytocin receptor in Sca-1+ cells. Oxytocin receptor mRNA was present at low levels in Sca-1+ cells before oxytocin treatment (Fig. 6, *lane P*). Expression levels of oxytocin receptor remained low in cells cultured with vehicle (Fig. 6, *lane V*). After treatment with oxytocin, expression levels of oxytocin receptor were up-regulated (Fig. 6, *lane OT*). In accordance with the inhibitory effect of oxytocin antagonist on oxytocin-induced cardiac differentiation, oxytocin antagonist inhibited oxytocin-induced up-regulation of the oxytocin receptor (Fig. 6, *lane OT+OTA*). These results suggest that the positive feedback mechanism, namely oxytocin-induced up-regulation of oxytocin receptor, plays an important role in oxytocin-induced cardiomyocyte differentiation of cardiac Sca-1+ cells.

Sca-1+ Cells Can Differentiate into Osteocytes and Adipocytes—It has been reported that Sca-1+ cells from skeletal muscle and bone marrow differentiate into various types of cells such as adipocytes, endothelial cells, muscle, neural, and hepatic cells (9, 11, 14). To determine whether the Sca-1+ cells from the adult murine heart have pluripotency, we examined whether these cells could differentiate into cells other than cardiomyocytes. When treated with osteogenic inducers, some of Sca-1+ cells were stained with alkaline phosphatase, one of the early markers of osteogenesis (Fig. 7*A*). RT-PCR clearly revealed that osteogenic marker mRNAs such as alkaline phosphatase and osteocalcin were induced in Sca-1+ cells after treatment with osteogenic inducers (Fig. 7*B*). On the other hand, Sca-1+ cells treated with oxytocin never expressed alkaline phosphatase and osteocalcin. When Sca-1+ cells were cultured with MDI-I mixture for twelve days, some of Sca-1+ cells showed cytoplasmic accumulation of oil droplets stained with Oil-Red O, indicating that Sca-1+ cells differentiated into adipocytes (Fig. 7*C*).

DISCUSSION

In this report, we have first demonstrated that adult cardiac Sca-1+ cells can differentiate into beating cardiomyocytes *in vitro* by treatment with oxytocin. When treated with oxytocin, the Sca-1+ cells expressed cardiac genes including Csx/Nkx-2.5, GATA4, MEF-2C, α-MHC, β-MHC, MLC-2a, MLC-2v, and cardiac α-actin, and cardiac proteins including GATA4, cardiac troponin T, tropomyosin, MLC-2v, sarcomeric myosin heavy chain, ANF, and connexin 43. Furthermore, some of Sca-1+ cells showed well organized sarcomere and spontaneous beating. Although transient treatment with 5′-azacytizine also induced expression of cardiac genes in Sca-1+ cells, it did not induce expression of cardiac troponin T, assembly of sarcomere or spontaneous beating. These results suggest that treatment with 5′-azacytizine induces differentiation of Sca-1+ cells into cardiomyocytes incompletely and that oxytocin is a more potent inducer of cardiac differentiation than 5′-azacytizine.

P19 teratocarcinoma cells differentiate into beating cardiomyocytes after treatment with Me_2SO and have been considered as a good model of *in vitro* cardiogenesis (34, 35). Several

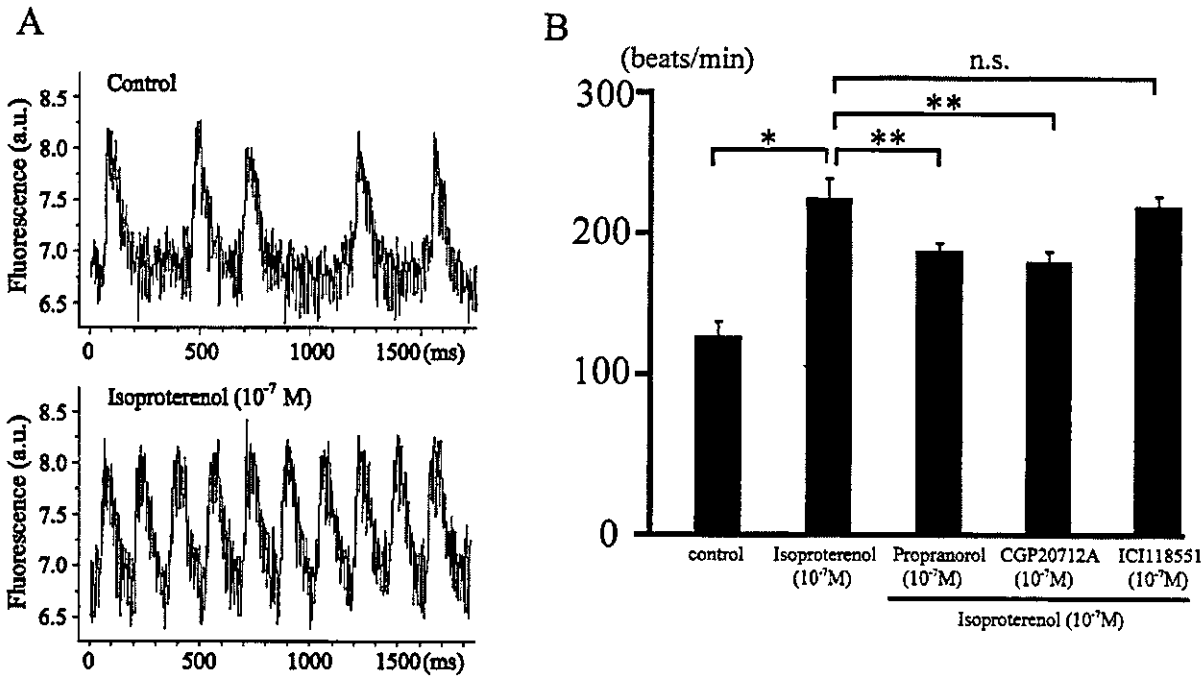

FIG. 5. **Physiological analysis of differentiated cardiac Sca-1+ cells.** *A*, $[Ca^{2+}]$, transients of beating cells derived from cardiac Sca-1+ cells before (*upper panel*) and after (*lower panel*) treatment with isoproterenol. *B*, the effects of subtype-specific β receptor blockers on isoproterenol-induced increase in beating rate of differentiated cardiac Sca-1+ cells. Preincubation with 10^{-7} M propranolol (nonselective β blocker) and 10^{-7} M CGP20712A (β_1-selective blocker) reduced isoproterenol-induced increase in beating rate significantly but 10^{-7} M ICI118551 (β_2-selective blocker) did not. *, $p < 0.01$ *versus* control; **, $p < 0.05$ *versus* isoproterenol only; *n.s.*, not significant.

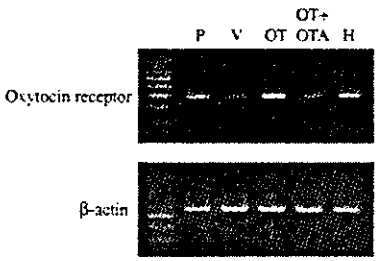

FIG. 6. **RT-PCR analysis of oxytocin receptor expression in Sca-1+ cells.** Oxytocin receptor mRNA was present at low levels in Sca-1+ cells before treatment (*lane P*). After oxytocin treatment, the oxytocin receptor mRNA expression was up-regulated (*lane OT*), but oxytocin antagonist inhibited oxytocin-induced oxytocin receptor up-regulation (*lane OT+OTA*).

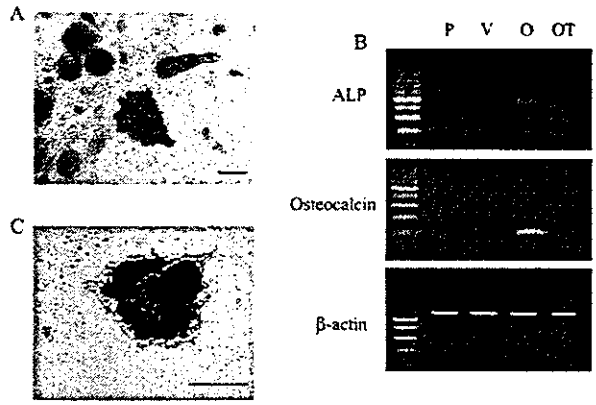

FIG. 7. **Osteogenic and adipogenic differentiation potential of Sca-1+ cells derived from the adult murine heart.** *A*, osteogenic differentiation of Sca-1+ cells was induced by treatment with ascorbic acid 2-phosphate, dexamethasone, and β-glycerophosphate for 3 weeks. Alkaline phosphatase staining (*blue*) was used for detection of osteocytes. *B*, RT-PCR experiment clearly revealed that osteogenic marker mRNAs such as alkaline phosphatase (*ALP*) and osteocalcin were induced in Sca-1+ cells by treatment with osteogenic inducers (*lane P* for pretreatment, *lane V* for vehicle treatment, *lane O* for osteogenic induction). Sca-1+ cells treated with oxytocin never expressed osteogenic marker mRNAs (*lane OT* for oxytocin treatment). β-actin was used as an internal control. *C*, adipogenic differentiation of Sca-1+ cells was induced by treatment with adipogenic mixture (MDI-I) for twelve days. Oil-Red O staining showed adipogenic differentiation of Sca-1+ cells. Hematoxylin was used for counterstaining of nuclei. *Bars*, 50 μm.

essential transcription factors in cardiomyogenesis such as GATA4 (34), Csx/Nkx-2.5 (34), and MEF-2C (36) are up-regulated in P19 cells treated with Me_2SO. Recently Paquin *et al.* (19) have reported that oxytocin induces P19 embryonic carcinoma cells to differentiate into cardiomyocytes. Treatment with oxytocin as well as with Me_2SO induced colony formation of beating cardiomyocytes, expression of cardiac proteins, and oxytocin receptor proteins. In this study, cardiac Sca-1+ cells expressed low levels of oxytocin receptor mRNA that were positively regulated by oxytocin itself, and pretreatment with oxytocin antagonist completely inhibited oxytocin-induced expression of cardiac genes. These results suggest that oxytocin induces cardiomyocyte differentiation of cardiac Sca-1+ cells through oxytocin receptors. Furthermore Sca-1+ cells treated with oxytocin did not express osteogenic marker mRNAs, suggesting that oxytocin is not a nonspecific inducer like 5′-azacytizine but has some specificity for cardiac lineage.

Oxytocin receptors are coupled to $G_{q/11}$ class GTP-binding proteins and stimulate the generation of inositol trisphosphate and diacylglycerol, leading to Ca^{2+} release and activation of protein kinase C (37). Oxytocin stimulates cell proliferation through calcium (38, 39) and protein kinase C pathways (38). Cassoni *et al.* (40) have reported that oxytocin stimulates cell

proliferation through oxytocin receptors that lead to an increase in intracellular Ca^{2+} and tyrosine phosphorylation. Tyrosine phosphorylation in oxytocin signaling has been reported to activate both p38 mitogen-activated protein kinase and extracellular signal-regulated kinase 2 (41, 42). The mechanism by which oxytocin stimulates tyrosine phosphorylation has not been elucidated, but may be mediated by $G\beta\gamma$ subunit dissociating from G_α subunit. Oxytocin inhibits the proliferation of human brain tumors (43), breast cancer cells (44), and adenocarcinoma of endometrium (45) via the cyclic adenosine monophosphate-protein kinase A pathway. Tahara *et al.* (46) have reported that the RhoA/Rho-kinase cascade is involved in oxytocin-induced rat uterine contraction. Among the considerable diversity of oxytocin-mediated signaling pathways, the specific pathway that activates cardiogenesis is currently unknown. Recently post-translational modification of cardiac transcription factors has been reported to be important for their transcriptional activities. Rho-like GTPases can phosphorylate GATA4 via activation of the p38 mitogen-activated protein kinase pathway, which enhances the potency of GATA4 (47). MEF2 is stimulated by calmodulin kinase activation in the heart (48). It remains to be determined which oxytocin signaling pathways are important for differentiation of cardiomyocytes.

It has been reported that c-kit+, Sca-1+, lineage-, and CD34-/low fraction of bone marrow cells contain hematopoietic stem cells, which contribute to long term multilineage reconstitution of the blood system in mice (49). Orlic *et al.* (50) and Gojo *et al.* (10) have reported that c-kit+ bone marrow cells and c-kit+ bone marrow-derived mesenchymal cells transdifferentiate into cardiomyocytes *in vivo*, suggesting that c-kit is one of the cell surface markers of multipotent stem cells in bone marrow. The multipotential stem cells also reside in skeletal muscle, although the origin of the stem cells is still controversial (51). Skeletal muscle-derived stem cells reported by Qu-Petersen *et al.* (11) and Torrente *et al.* (13) highly express CD34 and Sca-1 but not c-kit and CD45 and differentiate into neural and endothelial cells. In our study, cardiac Sca-1+ cells expressed low levels of c-kit, suggesting that the features of stem cell markers on cardiac stem cells is distinct from bone marrow-derived stem cells and rather similar to skeletal muscle-derived stem cells.

Tamaki *et al.* (14) isolated CD34+ and CD45− cells from the interstitial space of skeletal muscle, which highly expressed Sca-1 but not other endothelial progenitor cell markers. The CD34+/CD45− cells differentiated into adipocytes, endothelial and myogenic cells and expressed Bcrp1/ABCG2 gene mRNA, which is an important determinant of the SP phenotype. Recently Polesskaya *et al.* (52) have reported that CD45+/Sca-1+ cells from injured skeletal muscle differentiate into myoblasts much more than CD45−/Sca-1 cells. Because of the hematopoietic restricted expression of CD45 antigen, skeletal myogenic CD45+/Sca-1+ cells might be of hematopoietic origin. In our study, cardiac Sca-1+ cells expressed low levels of CD34 and ~40% of the cardiac Sca-1+ cells expressed CD45, one of hematopoietic cell markers. We sorted cardiac Sca-1+ cells on the basis of CD45 expression and cultured them with oxytocin. Some Sca-1+/CD45− cells expressed sarcomeric myosin after oxytocin treatment, but no Sca-1+/CD45+ cells expressed myosin (data not shown), suggesting that Sca-1+ cells that can differentiate into cardiomyocytes are in the CD45− population. Therefore, in terms of the expression of CD34 and CD45, the cardiac muscle stem cells are distinct from the previously reported skeletal muscle-derived stem cells.

Sca-1+ cells from the adult heart expressed GATA4 and Csx/Nkx-2.5, but not Oct-3/4 before treatment with oxytocin (data not shown), suggesting that the Sca-1+ cells are committed to cardiomyocytes to some degree. Makino *et al.* (24) have reported that mouse bone marrow-derived mesenchymal stem cells (CMG cells) differentiate into cardiomyocyte after 5′-azacytizine treatment. Although the cell surface antigens of CMG cells were not analyzed, the bone marrow-derived mesenchymal stem cells, which differentiated into cardiomyocytes after 5′-azacytizine treatment *in vivo*, expressed Sca-1, c-kit, and CD34 (10), suggesting that the cardiac Sca-1+ cells are different from bone marrow-derived mesenchymal stem cells. Cardiac Sca-1+ cells differentiated into osteocytes and adipocytes in appropriate conditions, suggesting that cardiac Sca-1+ cells have the intragerm layer multipotency. It remains to be determined whether the cardiac Sca-1+ cell population contains stem cells capable of differentiating to extra germ layer lineage.

The spontaneously beating differentiated cardiac Sca-1+ cells showed $[Ca^{2+}]_i$ transients and treatment with isoproterenol increased the frequency of $[Ca^{2+}]_i$ transients and beating rate. The similar response to isoproterenol has been reported in adult murine cardiomyocytes (53), embryonic stem cells-derived cardiomyocytes (54), and CMG cells (55). The β_1-selective blocker, CGP20712A, significantly reduced isoproterenol-induced increase in beating rate to the same extent as the non-selective β-blocker, propranolol, but the β_2-selective blocker, ICI118551, did not. These results suggest that the β_1 receptor is the predominant subtype that mediates the changes in beating rate of cardiomyocytes derived from Sca-1+ cells.

During the preparation of this article, two studies on cardiac stem cells were reported (56, 57). They have shown that c-kit+ or Sca-1+ cells derived from the adult murine heart express cardiac genes and proteins after the cardiogenic induction. We showed for the first time that there are potential adult cardiac stem cells that have an ability to proliferate and differentiate into various types of cells including beating cardiomyocytes *in vitro*. Although the role of cardiac stem cells is uncertain, our results suggest their possible role in cardiac repair. In addition, the understanding of precise molecular mechanisms of the differentiating process of cultured cardiac stem cells may provide us with new insights into cardiac development and regeneration.

Acknowledgments—We thank A. Ohkubo, R. Kobayashi, E. Fujita, M. Watanabe, M. Iida, and Y. Ohtsuki for technical assistance.

REFERENCES

1. Kajstura, J., Leri, A., Finato, N., Di Loreto, C., Beltrami, C. A., and Anversa, P. (1998) *Proc. Natl. Acad. Sci. U. S. A.* **95,** 8801–8805
2. Leri, A., Barlucchi, L., Limana, F., Deptala, A., Darzynkiewicz, Z., Hintze, T. H., Kajstura, J., Nadal-Ginard, B., and Anversa, P. (2001) *Proc. Natl. Acad. Sci. U. S. A.* **98,** 8626–8631
3. Beltrami, A. P., Urbanek, K., Kajstura, J., Yan, S. M., Finato, N., Bussani, R., Nadal-Ginard, B., Silvestri, F., Leri, A., Beltrami, C. A., and Anversa, P. (2001) *N. Eng. J. Med.* **344,** 1750–1757
4. Quaini, F., Urbanek, K., Beltrami, A. P., Finato, N., Beltrami, C. A., Nadal-Ginard, B., Kajstura, J., Leri, A., and Anversa, P. (2002) *N. Eng. J. Med.* **346,** 5–15
5. Anversa, P., and Nadal-Ginard, B. (2002) *Nature* **415,** 240–243
6. Asakura, A., and Rudnicki, M. A. (2002) *Exp. Hematol.* **30,** 1339–1345
7. Hierlihy, A. M., Seale, P., Lobe, C. G., Rudnicki, M. A., and Megeney, L. A. (2002) *FEBS Lett.* **530,** 239–243
8. van der Rijn, M., Heimfeld, S., Spangruade, G. J., and Wiessman, I. L. (1989) *Proc. Natl. Acad. Sci. U. S. A.* **86,** 4634–4638
9. Okumoto, K., Saito, T., Hattori, E., Ito, J. I., Adachi, T., Takeda, T., Sugahara, K., Watanabe, H., Saito, K., Togashi, H., and Kawata, S. (2003) *Biochem. Biophys. Res. Commun.* **304,** 691–695
10. Gojo, S., Gojo, N., Takeda, Y., Mori, T., Abe, H., Kyo, S., Hata, J., and Umezawa, A. (2003) *Exp. Cell Res.* **288,** 51–59
11. Qu-Petersen, Z., Deasy, B., Jankowski, R., Ikezawa, M., Cummins, J., Pruchnic, R., Mytinger, J., Cao, B., Gates, C., Wernig, A., and Huard, J. (2002) *J. Cell Biol.* **157,** 851–864
12. Asakura, A., Seale, P., Girgis-Gabardo, A., and Rudnicki, M. A. (2002) *J. Cell Biol.* **159,** 123–134
13. Torrente, Y., Tremblay, J. P., Pisati, F., Belicchi, M., Rossi, B., Sironi, M., Fortunato, F., El Fahime, M., D'Angelo, M. G., Caron, N. J., Constantin, G., Paulin, D., Scarlato, G., and Bresolin, N. (2001) *J. Cell Biol.* **152,** 335–348

14. Tamaki T., Akatsuka, A., Ando, K., Nakamura, Y., Matsuzawa, H., Hotta, T., Roy, R. R., and Edgerton, V. R. (2002) *J. Cell Biol.* **157,** 571–577
15. Schultheiss, T. M., Burch, J. B., and Lassar, A. B. (1997) *Genes Dev.* **11,** 451–462
16. Sugi, Y., and Lough, J. (1995) *Dev. Biol.* **168,** 567–574
17. Pandur, P., Lasche, M., Eisenberg, L. M., and Kuhl, M. (2002) *Nature* **418,** 636–641
18. Eisenberg, C. A., Gourdie, R. G., and Eisenberg, L. M. (1997) *Development* **124,** 525–536
19. Paquin, J., Danalache, B. A., Jankowski, M., McCann, S. M., and Gutkowska, J. (2002) *Proc. Natl. Acad. Sci. U. S. A.* **99,** 9550–9555
20. Mukaddam-Daher, S., Jankowski, M., Wang, D., Menaouar, A., and Gutkowska, J. (2002) *J. Endocrinol.* **175,** 211–216
21. Yao, A., Kohmoto, O., Oyama, T., Sugishita, Y., Shimizu, T., Harada, K., Matsui, H., Komuro, I., Nagai, R., Matsuo, H., Serizawa, T., Maruyama, T., and Takahashi, T. (2003) *Circ. J.* **67,** 83–90
22. Komuro, I., and Izumo, S. (1993) *Proc. Natl. Acad. Sci. U. S. A.* **90,** 8145–8149
23. Brunskill, E. W., Witte, D. P., Yutzey, K. E., and Potter, S. S. (2001) *Dev. Biol.* **235,** 507–520
24. Swanson, B. J., Jack, H. M., and Lyons, G. E. (1998) *Mol. Immunol.* **35,** 445–458
25. Robbins, J., Gulick, J., Sanchez, A., Howles, P., and Doetschman, T. (1990) *J. Biol. Chem.* **265,** 11905–11909
26. Kubalak, S. W., Miller-Hance, W. C., O'Brien, T. X., Dyson, E., and Chien, K. R. (1994) *J. Biol. Chem.* **269,** 16961–16970
27. Makino, S., Fukuda, K., Miyoshi, S., Konishi, F., Kodama, H., Pan, J., Sano, M., Takahashi, T., Hori, S., Abe, H., Hata, J., Umezawa, A., and Ogawa, S. (1999) *J. Clin. Investig.* **103,** 697–705
28. Asakura, A., Komaki, M., and Rudnicki, M. A. (2001) *Differentiation* **68,** 245–253
29. Zur Nieden, N. I., Kempka, G., and Ahr, H. J. (2002) *Differentiation* **71,** 18–27
30. Bi, W., Drake, C. J., and Schwarz, J. J. (1999) *Dev. Biol.* **211,** 255–267
31. Yao, A., Su, Z., Nonaka, A., Zubair, I., Spitzer, K. W., Bridge, J. H., Muelheims, G., Ross, J. Jr., and Barry, W. H. (1998) *Am. J. Physiol.* **275,** H1441-H1448
32. Jaiswal, N., Haynesworth, S. E., Caplan, A. I., and Bruder, S. P. (1997) *J. Cell Biochem.* **64,** 295–312
33. Limana, F., Urbanek, K., Chimenti, S., Quaini, F., Leri, A., Kajstura, J., Nadal-Ginard, B., Izumo, S., and Anversa, P. (2002) *Proc. Natl. Acad. Sci. U. S. A.* **99,** 6257–6262
34. Monzen, K., Shiojima, I., Hiroi, Y., Kudoh, S., Oka, T., Takimoto, E., Hayashi, D., Hosoda, T., Habara-Ohkubo, A., Nakaoka, T., Fujita, T., Yazaki, Y., and Komuro, I. (1999) *Mol. Cell. Biol.* **19,** 1096–1105
35. Hiroi, Y., Kudoh, S., Monzen, K., Ikeda, Y., Yazaki, Y., Nagai, R., and Komuro, I. (2001) *Nat. Genet.* **28,** 276–280
36. Skerjanc, I. S., Petropoulos, H., Ridgeway, A. G., and Wilton, S. (1998) *J. Biol. Chem.* **273,** 34904–34910
37. Hoare, S., Copland, J., Strakova, Z., Ives, K., Jeng, Y. J., Hellmich, M. R., and Soloff, M. S. (1999) *J. Biol. Chem.* **274,** 28682–28689
38. Thibonnier, M., Conarty, D. M., Preston, J. A., Plesnicher, C. L., Dweik, R. A., and Erzurum, S. C. (1999) *Endocrinology* **140,** 1301–1309
39. Tahara, A., Tsukada, J., Tomura, Y., Wada, K., Kusayama, T., Ishii, N., Yatsu, T., Uchida, W., and Tanaka, A. (2000) *Br. J. Pharmacol.* **129,** 131–139
40. Cassoni, P., Sapino, A., Munaron, L., Deaglio, S., Chini, B., Graziani, A., Ahmed, A., and Bussolati, G. (2001) *Endocrinology* **142,** 1130–1136
41. Ohmichi, M., Koike, K., Nohara, A., Kanda, Y., Sakamoto, Y., Zhang, Z. X., Hirota, K., and Miyake, A. (1995) *Endocrinology* **136,** 2082–2087
42. Strakova, Z., Copland, J. A., Lolait, S. J., and Soloff, M. S. (1998) *Am. J. Physiol.* **274,** E634–641
43. Cassoni, P., Sapino, A., Stella, A., Fortunati, N., and Bussolati, G. (1998) *Int. J. Cancer* **77,** 695–700
44. Cassoni, P., Fulcheri, E., Carcangiu, M. L., Stella, A., Deaglio, S., and Bussolati, G. (2000) *J. Pathol.* **190,** 470–477
45. Cassoni, P., Sapino, A., Fortunati, N., Munaron, L., Chini, B., and Bussolati, G. (1997) *Int. J. Cancer* **72,** 340–344
46. Tahara, M., Morishige, K., Sawada, K., Ikebuchi, Y., Kawagishi, R., Tasaka, K., and Murata, Y. (2002) *Endocrininology* **143,** 920–929
47. Wei, L., Roberts, W., Wang, L., Yamada, M., Zhang, S., Zhao, Z., Rivkees, S. A., Schwartz, R. J., and Imanaka-Yoshida, K. (2001) *Development* **128,** 2953–2962
48. Passier, R., Zeng, H., Frey, N., Naya, F. J., Nicol, R. L., McKinsey, T. A., Overbeek, P., Richardson, J. A., Grant, S. R., and Olson, E. N. (2000) *J. Clin. Investig.* **105,** 1395–1406
49. Osawa, M., Hanada, K., Hamada, H., and Nakauchi, H. (1996) *Science* **273,** 242–245
50. Orlic, D., Kajstura, J., Chimenti, S., Jakoniuk, I., Anderson, S. M., Li, B., Pickel, J., Mckay, R., Nadal-Ginard, B., Bodine, D. M., Leri, A., and Anversa, P. (2001) *Nature* **410,** 701–705
51. McKinney-Freeman, S. L., Jackson, K. A., Camargo, F. D., Ferrari, G., Mavilio, F., and Goodell, M. A. (2002) *Proc. Natl. Acad. Sci. U. S. A.* **99,** 1341–1346
52. Polesskaya, A., Seale, P., and Rudnicki, M. A. (2003) *Cell* **113,** 841–852
53. Lu, S., Hoey, A. (1998) *J. Mol. Cell Cardiol.* **32,** 143–152
54. Wobus, A. M., Wallukat, G., and Hescheler, J. (1991) *Differentiation* **48,** 173–182
55. Hakuno, D., Fukuda, K., Makino, S., Konishi, F., Tomita, Y., Manabe, T., Suzuki, Y., Umezawa, A., and Ogawa, S. (2002) *Circulation* **105,** 380–386
56. Beltrami, A. P., Barlucchi, L., Torella, D., Baker, M., Limana, F., Chimenti, S., Kasahara, H., Rota, M., Musso, E., Urbanek, K., Leri, A., Kajstura, J., Nadal-Ginard, B., and Anversa, P. (2003) *Cell* **114,** 763–776
57. Oh, H., Bradfute, S. B., Gallardo, T. D., Nakamura, T., Gaussin, V., Mishina, Y., Pocius, J., Michael, L. H., Behringer, R. R., Garry, D. J., Entman, M. L., and Schneider, M. D. (2003) *Proc. Natl. Acad. Sci. U. S. A.* **100,** 12313–12318